PNAS RESEARCH ARTICLE | DEVELOPMENTAL BIOLOGY

Tctp, a unique Ing5-binding partner, inhibits the chromatin binding of Enok in *Drosophila*

Lee-Hyang Kim[a,b,1], Ja-Young Kim[a,b,1], Yu-Ying Xu[a,b], Mi Ae Lim[c], Bon Seok Koo[c], Jung Hae Kim[a,b], Sung-Eun Yoon[d], Young-Joon Kim[e], Kwang-Wook Choi[f], Jae Won Chang[c,2], and Sung-Tae Hong[a,b,2]

Edited by Hugo Bellen, Baylor College of Medicine, Houston, TX; received October 29, 2022; accepted February 26, 2023

The MOZ/MORF histone acetyltransferase complex is highly conserved in eukaryotes and controls transcription, development, and tumorigenesis. However, little is known about how its chromatin localization is regulated. Inhibitor of growth 5 (ING5) tumor suppressor is a subunit of the MOZ/MORF complex. Nevertheless, the in vivo function of ING5 remains unclear. Here, we report an antagonistic interaction between *Drosophila* Translationally controlled tumor protein (TCTP) (Tctp) and ING5 (Ing5) required for chromatin localization of the MOZ/MORF (Enok) complex and H3K23 acetylation. Yeast two-hybrid screening using Tctp identified Ing5 as a unique binding partner. In vivo, Ing5 controlled differentiation and down-regulated epidermal growth factor receptor signaling, whereas it is required in the Yorkie (Yki) pathway to determine organ size. *Ing5* and *Enok* mutants promoted tumor-like tissue overgrowth when combined with uncontrolled Yki activity. Tctp depletion rescued the abnormal phenotypes of the *Ing5* mutation and increased the nuclear translocation of Ing5 and chromatin binding of Enok. Nonfunctional Enok promoted the nuclear translocation of Ing5 by reducing Tctp, indicating a feedback mechanism between Tctp, Ing5, and Enok to regulate histone acetylation. Therefore, Tctp is essential for H3K23 acetylation by controlling the nuclear translocation of Ing5 and chromatin localization of Enok, providing insights into the roles of human TCTP and ING5-MOZ/MORF in tumorigenesis.

Tctp | Ing5 | MOZ/MORF/Enok | histone acetylation | tumor reversion

In eukaryotes, epigenetic modifications on chromatin are important to regulate gene expression and maintain various physiological processes, such as cell development, fate determination, differentiation, and proliferation. Histone acetylation is a major chromatin modification, and its misregulation results in human diseases, such as cancer and developmental disorders (1, 2). Histone acetylation is catalyzed by histone acetyltransferase (HAT) enzymes, with more than 20 identified mammalian HATs classified into four families: GCN5/PCAF, p300/CREB-binding protein (CBP), Steroid receptor coactivator (SRC), and MOZ/Ybf2/Sas2/TIP60 (MYST) (2, 3). MOZ and MORF (MOZ/MORF) are MYST family HATs with high similarities in amino acid sequences and domain organization. Mammalian MOZ participates in cell cycle arrest (4, 5), stem cell maintenance (6), hematopoiesis, and development (7, 8), while MORF is important for bone cell formation (9). Mutations of MOZ/MORF result in various human diseases, including cancers and congenital malformations of the brain, head, and heart (2, 3, 10). *Drosophila* Enok, a human MOZ/MORF homolog, also regulates various in vivo functions, including the formation of brain neuroblasts (11), retinal axon wiring (12), egg development (13, 14), DNA replication (15), gene transcription (14, 16, 17), and germline genome stability (18). Despite the important roles of MOZ/MORF/Enok, the factors regulating their chromatin localization are poorly understood.

As a catalytic subunit, MOZ/MORF forms a HAT protein complex with the subunits BR140, EAF6, and inhibitor of growth 5 (ING5). *Drosophila* Enok also forms a HAT protein complex with similar subunit homologs (15). BR140 is a scaffold protein (10, 19) that preferentially resides in the cytoplasm and modulates the in vitro substrate specificity of HAT (15). EAF6 is the smallest subunit and translocates to the nucleus with BR140 in human cell lines (19). ING5 binds to BR140 and enhances MOZ/MORF activity for histone acetylation and target gene expression (10, 19, 20). Human ING5 belongs to the ING family of tumor suppressors that control the cell cycle, cell growth, and apoptosis (21, 22), and its misregulation or mutation is associated with various human cancers (23–27). ING5 interacts with the P53 pathway (28); however, its relevance in other signaling pathways is relatively less studied (22, 28, 29).

In human colorectal cell lines, Moz is required for Yes-associated protein (YAP) expression (a human Yki homolog) (30). MORF mutation in a patient with Noonan syndrome induces the increased activity of Extracellular signal-regulated kinase (ERK) Mitogen-activated protein kinase (MAPK) signaling (31). Recently, it has been reported that ING5 overexpression

Significance

Body formation, organ development, and size determination are critical processes regulated by histone acetylation. In *Drosophila* and humans, acetylation on histones is performed by Monocytic leukemia zinc finger protein (MOZ)/MOZ-related factor (MORF) acetyltransferase. Defects in MOZ/MORF drive developmental disorders or cancer progression. The key unresolved questions about MOZ/MORF function are: What controls its function? Furthermore, how does it regulate the MOZ/MORF function? Numerous studies have revealed MOZ/MORF's roles; however, its regulatory mechanism is less understood. Here, we report that in *Drosophila*, Tctp (Translationally controlled tumor protein) protein, a unique binding partner of fly MOZ/MORF, negatively controls MOZ/MORF function, thereby inhibiting uncontrolled histone H3K23 acetylation. The results of this study enhance our understanding of body/organ formation control and its role in human diseases, including cancers and developmental disorders.

The authors declare no competing interest.

This article is a PNAS Direct Submission.

[1]L.-H.K. and J.-Y.K. contributed equally to this work.

[2]To whom correspondence may be addressed. Email: strive1005@hanmail.net or mogwai@cnu.ac.kr.

This article contains supporting information online at https://www.pnas.org/lookup/suppl/doi:10.1073/pnas.2218361120/-/DCSupplemental.

Published April 4, 2023.

in glioblastoma stem cells induces ERK phosphorylation (26). However, a detailed in vivo or genetic study on the interaction between ING5/MOZ/MORF and the epidermal growth factor receptor (EGFR) or Yki pathway is lacking.

In human cell lines, ING5 exists both in the cytoplasm and the cell nucleus (25, 32) and interacts with two HAT protein complexes (MOZ/MORF and HBO1) to regulate gene transcription by affecting histone H3 or H4 acetylation (20). ING5 is critical for the differentiation of epithelium and neurons from cultured cells (26, 33). However, our understanding of its in vivo functions is limited due to a lack of *Ing5*/*ING5*-null mutants (21). Whether ING5 regulates the chromatin binding of the MOZ/MORF complex in vivo and how its nuclear localization is regulated remain unclear.

Translationally controlled tumor protein (TCTP) is highly conserved in eukaryotes (34–36) and controls diverse biological processes, such as growth (37–39), mitosis (40, 41), survival (42, 43), protein synthesis (44), DNA repair (45, 46), cell adhesion (47), ion homeostasis (48), and immune responses (49). Human TCTP is up-regulated in various cancer cell lines, where it binds to MDM2, an inhibitor of the tumor suppressor P53, and promotes the degradation of P53 (40): TCTP upregulation has been implicated in tumorigenesis (34), while TCTP inhibition can induce tumor reversion by up-regulating P53 (35, 36, 50). Tumor reversion is a process suppressing tumor malignancy and is mainly regulated by TCTP–MDM2–P53 proteins in mammals. Interestingly, similar to P53, ING5 expression is decreased in cancer cell lines, and its overexpression can suppress tumor formation (28). However, the association between TCTP/Tctp and ING5 in tumorigenesis and tumor reversion is unknown.

Drosophila models have helped elucidate the in vivo functions of TCTP. *Drosophila* TCTP (Tctp) regulates organ growth (38, 39, 51, 52), stem cell regeneration (53), junction formation (47), genome stability (46, 54), and global gene expression (54). It also serves various epigenetic functions, including the regulation of 1) histone phosphorylation (γH2AX/H2Av) for DNA repair, 2) histone methylation (H3K9me2) for heterochromatin formation, and 3) chromatin remodeling for gene expression (35, 45, 46, 54). However, the epigenetic role of TCTP/Tctp on histone acetylation via HAT remains unknown.

This study demonstrates that Tctp binds directly to *Drosophila* ING5 (Ing5) and prevents its nuclear translocation, thereby inhibiting the function of the Ing5-Enok complex. We generated *Ing5*-null *Drosophila* mutants to investigate its in vivo functions and observed an essential role of Ing5 for proper differentiation in developing animals. Ing5 antagonistically interacted with Tctp to regulate the EGFR and Yorkie (Yki) pathways. *Ing5* and *Enok* knockdown combined with uncontrolled Yki activity elicited tumor-like tissue overgrowth, which was suppressed by Tctp depletion. We demonstrate that Tctp inhibits the nuclear translocation of Ing5 and chromatin binding of Enok, providing a mechanism for regulating histone H3 acetylation (H3K23Ac) by Tctp. Finally, we identified a feedback mechanism between Tctp, Ing5, and Enok in maintaining acetylation for proper differentiation. Our findings suggest that Tctp is a critical negative regulator of the Ing5-Enok complex that prevents uncontrolled H3K23 acetylation. We postulate that the nuclear localization of Ing5 through the depletion of Tctp could provide an alternative epigenetic pathway for tumor reversion, parallel to or independent of the TCTP–MDM2–P53 axis in humans (35, 36, 40).

Results

Physical Interaction between Tctp and Ing5. We previously performed a yeast two-hybrid screening of the *Drosophila* embryonic library using Tctp as a bait protein to find unique Tctp binding proteins (54) and identified a candidate binding partner in a partial protein of 232 amino acids encoded by the gene *CG9293* (Fig. 1*A*), a *Drosophila* homolog of human ING5 with ~58% protein sequence identity (Fig. 1*B* and *SI Appendix*, Fig. S1*H*). ING5 is a Type-II tumor suppressor protein whose expression is down-regulated in cancers (21). The ING family consists of three members in *Drosophila* and five in humans and contains two common domains: ING and plant homeodomain (PHD)-type zinc finger motifs (Fig. 1*B*) (21). However, *Drosophila* Ing5 has low sequence identity with Ing1 and Ing3 (Fig. 1*B*). Further, the wing phenotype produced by the knockdown of *Ing5* differed from

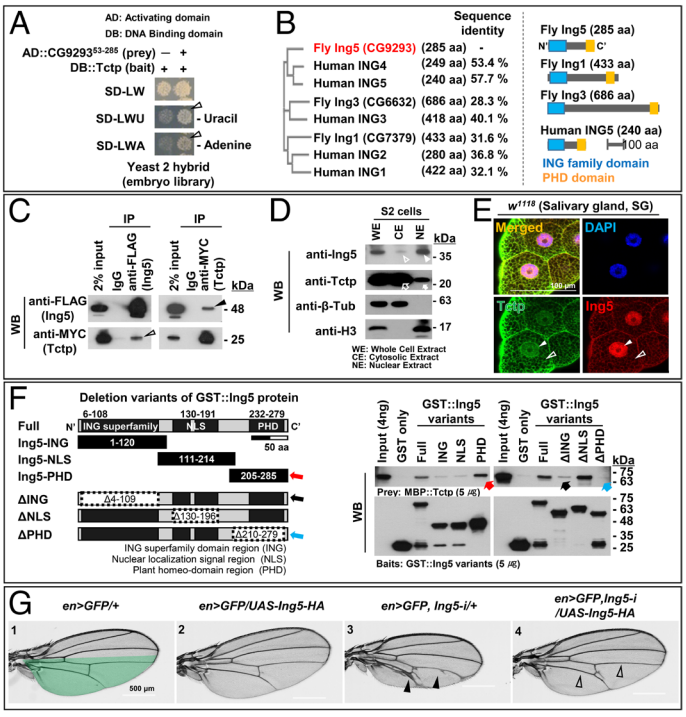

Fig. 1. Physical interaction between Tctp and Ing5 via the PHD motif. (*A*) Yeast two-hybrid assay. (Arrowheads) Direct interaction between Tctp bait and Ing5 prey proteins forms a functional Gal4, which activates the expression of selection markers (*URA3* and *ADE2*), allowing yeast transformants to grow on the selection medium SD-LWU (-uracil) or SD-LWA (-adenine). (*B*) (*Left*) Phylogenetic analysis of ING proteins from humans and *Drosophila*. Percent identities of amino acid (aa) sequences are shown on the *Right*. The ING family consists of 5 members in humans and 3 members in *Drosophila*. (*Right*) Human ING5 and fly Ing family members. (*C*) Reciprocal coimmunoprecipitation (co-IP). FLAG-tagged Ing5 was coimmunoprecipitated with MYC-tagged Tctp in S2 cell extracts (open arrowhead) and vice versa (closed arrowhead). (*D*) Western blots (WB) on fractionated cytosolic (CE) or nuclear extracts (NE) of S2 cells. WE, whole-cell extract. Both Ing5 and Tctp proteins coexist in CE and NE (arrowheads and arrows). Tctp was more abundant in CE (open arrow) than NE. β-tubulin and histone H3 are the loading and fractionation controls, respectively. (*E*) Colocalization of Tctp (green) and Ing5 (red) in cell nuclei and cytosol of salivary glands (SGs; closed and open arrowheads, respectively). Both proteins in the cytosol appear in a mesh-like pattern. (*F*) In vitro GST pull-down assay. (*Left*) Schematic domain structure of Ing5 and mutated Ing5 protein variants. The full-length Ing5 protein has three conserved domains (ING, NLS, and PHD). (Red arrows) Direct Tctp binding to the PHD domain fragment of the Ing5 protein (205 to 285 aa region). (Black and blue arrows) ING superfamily and PHD domains are required for direct binding to Tctp. (*G*) Adult phenotypes in *en>HA-tagged-Ing5* or *en>Ing5-RNAi* wings. Ing5 depletion in the posterior wing compartment (green) causes the formation of extra and thickened veins (closed arrowheads), which was rescued by Ing5 overexpression (open arrowheads).

that of other members (*SI Appendix*, Fig. S1 *A*–*G*), suggesting that *Ing5* has nonredundant functions from other *Ing* genes.

Coimmunoprecipitation (co-IP) using S2 cell extracts confirmed the physical interaction between Tctp and Ing5. When FLAG-tagged Ing5 was immunoprecipitated using FLAG antibody, MYC-tagged Tctp was found to coexist with Ing5 and vice versa (Fig. 1*C*), indicating that Ing5 and Tctp can form a protein complex. This direct binding between Tctp and Ing5 was supported by western blot analysis on fractionated S2 cell extracts, and by immunohistochemistry (IHC) in larval salivary glands (SGs) with large nuclei (Fig. 1 *D*–*E* and *SI Appendix*, Fig. S2). Tctp and Ing5 occurred in both cytosolic and nuclear extracts (Fig. 1*D*) and were colocalized in larval SGs in a similar pattern (Fig. 1*E*).

To identify the Ing5 protein domains required for direct binding to Tctp, we performed an in vitro pull-down assay between Maltose-binding protein (MBP)-tagged Tctp and GST-tagged Ing5 protein fragments containing a domain for ING superfamily, NLS, or PHD and observed that Tctp binds to the PHD domain fragment (Fig. 1*F*, red arrows). We examined the binding activity of GST-tagged Ing5 variants with a missing domain (ΔING, ΔNLS, or ΔPHD) and found no physical interaction between Tctp and ΔPHD (Fig. 1*F*, blue arrows), confirming that Tctp binds to Ing5 via its PHD domain. The ΔING variant also showed weak binding to Tctp protein, suggesting that the ING superfamily domain might be critical in maintaining the tertiary structure of Ing5 proteins (Fig. 1*F*, black arrows).

In some human tumor cell lines, ING5 overexpression inhibits proliferation and increases apoptosis (28). Thus, we hypothesized that the ectopic expression of Ing5 using the Gal4–Upstream activating sequence (UAS) system (55) could inhibit the growth of fly tissues, as shown for human ING5. Unexpectedly, ectopic Ing5 expression in the fly wing showed no growth inhibition (Fig. 1*G*-#2). Instead, *Ing5* knockdown in the developing wing led to a reduced wing size with extra and thickened veins in adults (Fig. 1*G*-#3 and *SI Appendix*, Fig. S1*G*), implying that Ing5 determines organ size or differentiation rather than proliferation.

Ing5 Is Required for Proper Differentiation Rather Than Cell Proliferation In Vivo. To elucidate the in vivo function of Ing5, we generated three deletion mutants for fly *Ing5* (Δ596, Δ700, and Δ1260) (Fig. 2*A*). Second instar larval *Ing5* homozygotes (Δ596 and Δ1260) were considered null mutants because they had no detectable Ing5 proteins compared to wild-type controls (w^{1118}) (Fig. 2*B*).

Hatched *Ing5*-null homozygotes developed normally until the second instar stage [3 d after egg deposit (AED)]. Although development was delayed from the early third instar (Fig. 2*C*, closed arrowheads), *Ing5*-null homozygote larvae reached a similar size to that of the controls and started pupation at ~6.5 d AED (Fig. 2*C*, open arrowheads; Fig. 2*D*, a plot in green). The final pupal length was comparable to that of the controls, but the width and volume were slightly reduced (Fig. 2*D*). *Ing5*-null homozygote growth was arrested at the prepupal stage, and all individuals died eventually (Fig. 2*C*, open arrowheads). Pupariation timing was impaired in both homozygous and heterozygous *Ing5*-null mutants (Fig. 2*D*, plots). Pupariation was delayed by ~1.5 d in *Ing5*-null

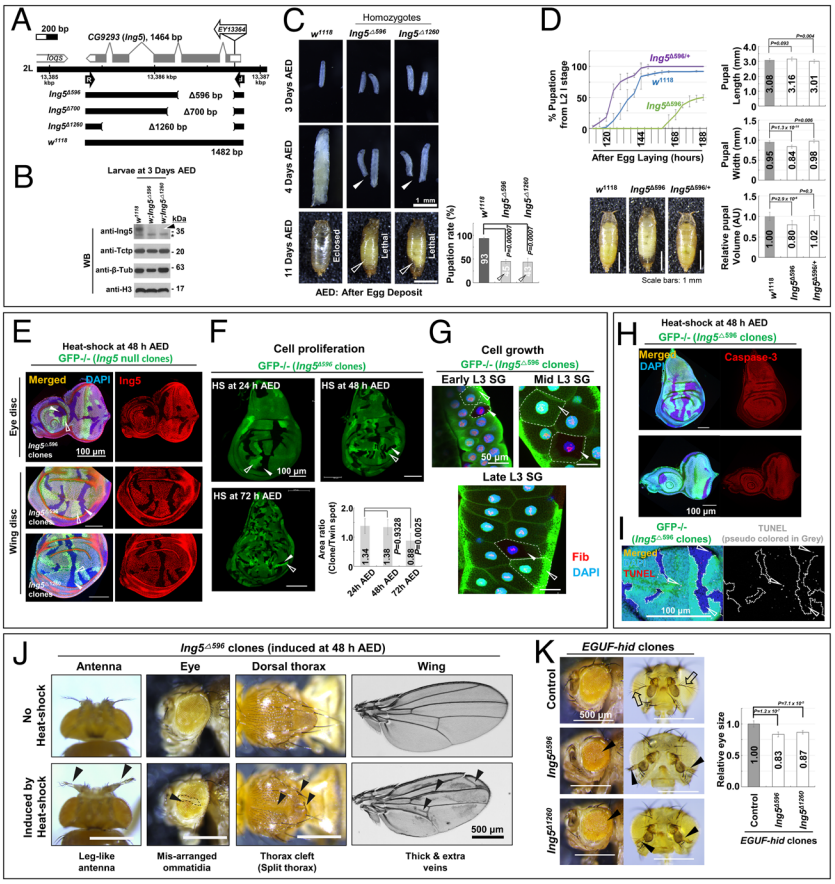

Fig. 2. The role of Ing5 in cell differentiation. (*A*) Imprecise excision of *EY13364* transposon (white arrow) at the 5′-UTR of the *CG9293* genomic locus produced *Ing5* deletion mutants, Δ596, Δ700, and Δ1260. A primer set for genomic PCR is indicated with black arrows. (*B*) No detection of Ing5 proteins in *Ing5Δ*^{596} and *Ing5Δ*^{1260} larval homozygotes (arrowhead). The asterisk indicates a nonspecific band in the western blot analysis (WB). β-tubulin and histone H3 are loading controls. Tctp level is intact in the *Ing5*-null mutants. (*C*) *Ing5* homozygotes showed a developmental delay from the early third instar stage (closed arrowheads) but eventually reached a size similar to that of the wild-type controls and developed to pupae (about 43 to 45%, open arrowheads). AED: after egg deposit. n = 60 larvae. (*D*) Pupation timing of *Ing5* mutants. *Ing5Δ*^{596} heterozygotes pupated ~10 h earlier (purple line, n = 115) than wild type (w^{1118}, blue line, n = 160), whereas *Ing5Δ*^{596} homozygotes showed a 1.5-d delay (green line, n = 42). *Ing5Δ*^{596} homozygote pupae (n = 38) were slightly slimmer than wild type (n = 43) or *Ing5Δ*^{596}/+ heterozygotes (n = 16). (*E*–*G*) Intact cell proliferation and growth rates in *Ing5*-null clones (GFP negative, closed arrowheads). Twin-spot clones are marked with an open arrowhead. (*E*) The similar sizes of *Ing5*-null and twin-spot clones in the developing eye or wing discs produced at 48 h AED (arrowheads). Ing5 (red) is not seen in the mutant clones. (*F*) *Ing5*-null clones (GFP negative, closed arrowheads) were generated at 24 h, 48 h, or 72 h AED and dissected at the late third instar stage. The measured area (representing cell proliferation rate) of the *Ing5*-null clones in wing discs was comparable to that of the twin-spot clones (histogram). n = 11 discs for 24 h, 21 discs for 48 h, and 16 discs for 72 h. (*G*) Cell growth rate in *Ing5Δ*^{596}-null clones. In SGs, *Ing5*-null clones (GFP negative, closed arrowheads) were induced at 6 h AED (early embryogenesis) and dissected from early, middle, or late third instar stage. Cell nuclei (blue) and nucleoli (red, fibrillarin) are seen. (*H* and *I*) Undetectable apoptosis in *Ing5*-null clones. (*H*) No activation of caspase-3 (red) in *Ing5 Δ*^{596}-null clones in the eye or wing discs. (*I*) TUNEL assay. No increase in apoptotic DNA fragmentation (red foci [pseudocolored in gray], open arrowheads) in *Ing5 Δ*^{596}-null clones (GFP negative) compared with the surrounding cells or twin-spot clones. (*J*) (*Bottom*) Abnormal development/fate determination in adults having *Ing5Δ*^{596}-null clones (arrowheads). (*Top*) The same genotype without heat-shock treatment has a normal phenotype. (*K*) EGUF-hid *Ing5*-null clones. The eyes and antenna, fully filled with *Ing5Δ*^{596} or *Ing5Δ*^{1260} mutation, show a reduced eye size, abnormal ommatidia array, and antenna-to-leg transformation (arrowheads). Arrow indicates the antenna of the control flies. For eye size quantification, ten eyes for each genotype were used.

homozygotes compared to the wild-type controls, whereas *Ing5Δ*$^{596/+}$ heterozygotes pupated approximately 10 h faster than the controls. Such defects in the prepupal stage and pupariation timing of *Ing5* mutants are similar to those of the *Enok*-null mutation (11). The retarded larval development and minimally affected pupal size in *Ing5*-null mutants suggest that the developmental defects might stem from abnormal differentiation or cell fate determination rather than defective cell proliferation/growth.

Consequently, we performed clonal analysis (56) to evaluate cell proliferation and growth in imaginal discs bearing *Ing5*-null clones (Δ596 or Δ1260, Fig. 2 *E–G*), but found no noticeable proliferation or growth defects in the eye and wing discs (generated at the second instar stage, 48 h AED) compared with the twin-spot clones (Fig. 2*E*). We further inspected cell proliferation and growth in the *Ing5*-null clones with more elaborate approaches. First, we induced mutant clones in wing discs at the first, second, or early third instar stage and examined cell proliferation at the late third instar stage. The relative cell proliferation ability of mutant and twin-spot clones was compared by measuring the ratio of mutant to twin-spot clonal area (Fig. 2*F*). Interestingly, the areas of *Ing5*-null clones, assessed at 24 h or 48 h AED, were larger than those of their twin-spot clones. Second, for cell growth analysis, *Ing5*-null clones were induced in SGs at the early stage of embryogenesis. An SG arises from ~100 cells during embryogenesis and grows by simply increasing cell volume without further cell division (57). When examined at the early, mid, or late third instar stage, the null and twin-spot clones showed similar cell sizes (Fig. 2*G*). Consistently, *Ing5*-null clones or knockdown tissues showed no defects in cell division (PH3), DNA replication (BrdU), cell number, cell size, cell–cell adhesion, and insulin signaling for cell growth (*SI Appendix*, Fig. S3 *A–H*). Overall, our findings suggest that the *Ing5* mutation causes no significant defects in cell proliferation and growth in fast-growing larval tissues.

Next, we tested whether the *Ing5*-null mutation causes defective differentiation or cell fate determination. To circumvent the lethality of null mutants during the pupal stages, we generated mitotic mutant clones of *Ing5Δ*^{596} at the second instar stage (48 h AED), which were reared to the adult stage. Adult flies with *Ing5* mutant clones showed various defects in differentiation and cell fate determination in different body structures, including antenna-to-leg homeotic transformation, disorganized ommatidial array, thorax cleft, and smaller wings with extra and thickened veins (Fig. 2*J*, arrowheads). The *Ing5*-null phenotypes in the eye and antenna were confirmed using the Eyeless-GAL4 UAS-FLP (EGUF)-hid method (58) for generating organs composed of exclusively mutant cells. The heads with EGUF-hid *Ing5*-null clones showed abnormal ommatidial arrangement, reduced eye size, and leg-like antennae with 100% penetrance (n = 85) (Fig. 2*K*). The smaller wings and eyes in adults with *Ing5*-null clones were unrelated to cell death (Fig. 2 *H* and *I*). These clonal analyses suggest that Ing5 is required for differentiation and cell fate determination in imaginal discs rather than cell proliferation and growth.

Enhanced EGFR Signaling Activity in *Ing5* Mutants. The EGFR pathway regulates vein formation in fly wing development (59). Since *Ing5*-mutant wings have extra and thickened vein phenotypes, we investigated the in vivo relationship between EGFR signaling and Ing5.

First, we tested whether vein phenotypes in *Ing5* mutants are genetically associated with EGFR pathway components. In the EGFR pathway, the ligand-activated EGFR transmits its signal to the Ras/Raf/ERK axis (60). In the nucleus, activated Rolled (Rl, *Drosophila* ERK) inhibits the transcriptional repressor Capicua (Cic) by phosphorylation. Simultaneously, the nuclear ERK phosphoactivates Pointed (pnt), a transcriptional activator, to promote the expression of downstream target genes (Fig. 3*B*-#1) (61). When we combined *en>Ing5-RNAi* with a copy of *EGFR* loss-of-function (LOF) allele (*Egfr*^{t2}) or *rl* deficiency allele (*rl*^{10a}), the abnormal venation in *Ing5-RNAi* wings was suppressed (Fig. 3*A*-#7–8). *rl-RNAi* (v109108) showed a similar phenotype (Fig. 3*A*-#9). *Egfr-*, *Ras-*, or *Raf-RNAi* also suppressed the abnormal venation in *en>Ing5-RNAi* wings (*SI Appendix*, Fig. S4*A*-#8–10, open arrowheads). Interestingly, we also found a no-vein phenotype in *Egfr-*, *Ras-*, *Raf-*, or *rl-RNAi* adult wings (*SI Appendix*, Fig. S4*A*-#2–6, black arrows), and apoptosis in strongly *rl*-knockdowned wing discs (*SI Appendix*, Fig. S4*C*, open arrowheads) was suppressed by additional *Ing5-RNAi* (*SI Appendix*, Fig. S4*A*-#8–12, open arrowheads; *SI Appendix*, Fig. S4*C*, closed arrowheads). These results suggest that EGFR signaling is involved in *Ing5*-knockdown vein phenotypes and that the *Ing5* mutation may increase EGFR signaling activity and cell survival.

In wing development, genes such as *Cic*, *ash2*, *net*, and *blistered* (*bs*) suppress EGFR signaling in intervein regions to restrict vein formation, and mutations in these genes cause extra and thickened venation in the intervein area due to increased EGFR signaling (59, 62–65). Accordingly, we assessed whether the ectopic vein phenotype in *en>ing5-RNAi* wings is enhanced by intervein gene mutations. Weak Cic depletion by P-element insertion or *Cic-RNAi* did not affect venation in adult wings (Fig. 3*B*-#2–3). However, Cic depletion synergistically enhanced abnormal vein formation in *Ing5*-knockdown wings (Fig. 3*B*-#6–7, black arrowheads). By contrast, PCV loss by Cic overexpression (*en>Cic*^{F001848}) was suppressed by *Ing5-RNAi* (Fig. 3*B*-#4 and 8). Other intervein mutants, such as *ash2*^{1}, *net*^{1}, or *bs*^{k07909}, showed similar genetic interaction with *Ing5-RNAi*, promoting abnormal venation in *en>Ing5-RNAi* wings (*SI Appendix*, Fig. S4*B*-#6–9). These synergistic genetic interactions between *Ing5*-knockdown and intervein mutants suggest that Ing5 is highly related to suppressors of EGFR signaling. In addition, since Cic, net, and bs are key downstream inhibitors of EGFR signaling (62–65), the results suggest that Ing5 has an inhibitory role downstream of EGFR signaling.

Compared to EGFR overexpression (Fig. 3*A*-#5 and 10, black arrowhead), intervein gene mutations had a stronger effect on abnormal vein phenotype in *en>Ing5-RNAi* wings (Fig. 3*B*-#6–7 and *SI Appendix*, Fig. S4*B*-#6–8). Consequently, we investigated the effect of Ing5 depletion on the expression of EGFR target genes or intervein genes (Fig. 3 *C–F*). We used *pnt-GFP* or *argos(aos)-lacZ* reporter to detect EGFR signaling activity and *net-GFP* or *bs-lacZ* to detect intervein gene expression. First, we assessed the effect of *Ing5* knockdown on EGFR reporter activity in the dorsal compartment of wing discs using *ap-Gal4*. *ap>Ing5-RNAi* discs showed moderately increased EGFR signaling (Fig. 3 *C* and *D*). *pnt-GFP* expression was mildly up-regulated in the dorsal proveins of *ap>Ing5-i* discs compared with its ventral proveins or *ap-Gal4*/+ control (Fig. 3*C*, open arrowhead). Unlike the control discs, *ap>Ing5-RNAi* discs showed ectopic *pnt-GFP* expressions in the notum, dorsal hinge, and anterior dorsal wing margin (Fig. 3*C*, open arrows). Another EGFR target gene reporter, *aos-lacZ*, also showed increased expression in the dorsal hinge, notum, and proveins of *ap>Ing5-RNAi* wing discs (Fig. 3*D*, open arrowheads and arrow) compared with *ap>GFP*/+ control discs (Fig. 3*D*). Next, we examined whether *Ing5* knockdown reduces intervein reporter expression to increase EGFR activity indirectly. Notably, *net-GFP* or *bs-lacZ* expression was considerably suppressed by *ap>Ing5-RNAi* (Fig. 3 *E* and *F*, open arrowheads) compared with its internal control or *ap-Gal4*/+ discs. Altogether, our findings suggest that Ing5 inhibits EGFR signaling for cell survival and venation by activating a subset of negative regulators.

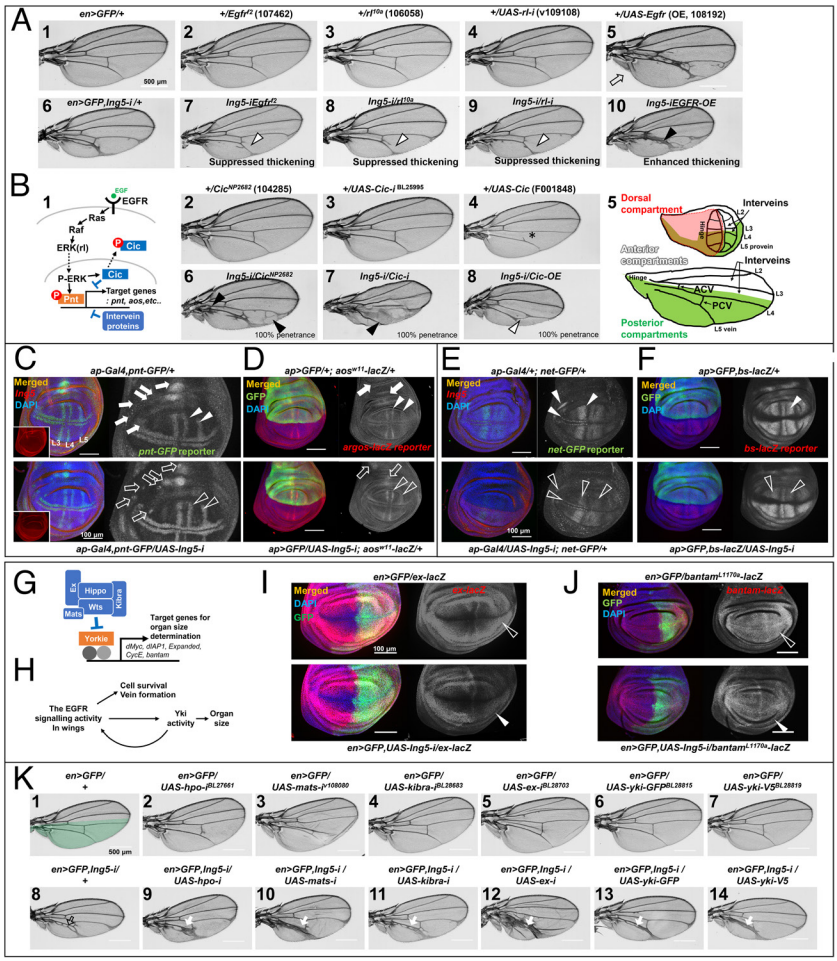

Fig. 3. Enhanced EGFR and reduced Yki signaling in *Ing5* mutants. (*A*–*F*) Enhanced EGFR signaling in *Ing5* mutants. (*A*) Genetic interaction between *Ing5-RNAi* and EGFR signaling components. The EGFR pathway is depicted in panel *B1*. (White arrowheads) Abnormal venation in *en>Ing5-RNAi* wings was suppressed by adding *rl-RNAi* or reducing the gene dosage for *Egfr* ($Egfr^{f2}$/+) or *rolled* (rl^{10a}/+). (Black arrowhead) EGFR overexpression enhanced the *Ing5-RNAi* vein phenotype. The small wing size of *en>Ing5-RNAi* was not restored by increased EGFR activity. (*B*) Genetic interaction between *Ing5-RNAi* and intervein gene mutants. (#2-3) Normal venation in *En-Gal4* wings containing a P-element insertion (*NP2682*) or *Cic-RNAi*. (#6-7, black arrowheads) Phenotypes in *en>Ing5-RNAi* wings synergistically interact with *Cic*-reduced wings, resulting in extra and thickened vein formation. (#4, #8) Suppressed PCV formation by Cic overexpression (asterisk) is rescued by additional *Ing5-RNAi* (white arrowhead). (#5) Schematic drawings of wing tissues. (*C*–*F*) *pnt-GFP* and *aos-lacZ* reporters for EGFR signaling are mainly expressed in proveins and hinge regions (*C* and *D*, *Upper*). *net-GFP* and *bs-lacZ* reporters are expressed in intervein regions (*E* and *F*, *Upper*). GFP-positive or Ing5-negative signal marks the dorsal compartment expressing *ap-Gal4*. (*C* and *D*) *ap>Ing5-i* moderately enhanced EGFR signaling activity in dorsal proveins (open arrowheads). Ectopic *pnt-GFP* or *aos-lacZ* expression (foci) by *Ing5-RNAi* is also seen in the notum, dorsal hinge, and anterior wing margin (open arrows). (*E* and *F*) Strong reduction of intervein gene expression (*net-GFP* or *bs-lacZ*) by *Ing5-RNAi* (open arrowheads). (*G*–*K*) Reduced Yki activity in *Ing5* mutants. (*G*) The Hippo (Hpo) tumor suppressor pathway. Hpo, Wts, Mats, Kibra, or Ex protein inhibits Yki activity to adequately regulate organ/tissue size. Yki activates its target gene expression (dMyc, dIAP1, Ex, cyclin E (CycE), and bantam). (*H*) The EGFR signaling controls vein formation, cell survival, and organ size in wings. To regulate wing size, the EGFR pathway can interact with Yki—mutually activating each other. (*I* and *J*) Reduced expression of Yki activity reporters. LacZ reporter expression of *ex* or *bantam* was reduced in *en>Ing5-RNAi* wing discs (closed arrowheads) compared to control discs (open arrowheads). (*K*) *En-Gal4*-driven knockdown of hpo, mats, kibra, or ex enlarges adult wing size (#2–5) by increasing Yki activity, compared to *en-Gal4* controls (#1). Yki overexpression also resulted in wing size expansion (#6 and 7). Increasing Yki activity in *en>Ing5-RNAi* wings restored the wing size reduction (#8–14). Since Yki activity can increase EGFR activity (panel *H*), vein formation in *en>Ing-RNAi* (#8, open arrow) was enhanced by up-regulated Yki activity (#9–14, white arrows).

Reduced Yki Activity and Organ Size in *Ing5* Mutants. Enhancing EGFR activity can increase adult wing size (Fig. 3*A*-#5, open arrow) (59, 66–71). The abnormal venation in *en>Ing5-RNAi* wings results from enhanced EGFR activity; however, a decrease in wing size was observed in a single mutant of *Ing5*, double mutants of *Ing5* and *EGFR/Ras/Raf/rl* genes, and *Ing5* mutants coexpressing the ectopic *EGFR* transgene (Fig. 3*A* and *SI Appendix*, Fig. S4*A*). Thus, we assessed whether Ing5 mutations could impair the Hippo/Yki pathway.

In *Drosophila*, the Hippo tumor suppressor pathway controls organ size by inhibiting the transcriptional activator Yki. Yki activates the expression of various target genes, including *dMyc*, *DIAP1*, *Cyclin E (CycE)*, *bantam*, and *Expanded (ex)*, to increase organ size (Fig. 3*G*) (72). Besides wing vein formation, the ectopically induced EGFR pathway can enhance Yki activity to increase wing size (Fig. 3*H*) (70). Therefore, we hypothesized that the reduced wing size in *Ing5* mutants could be related to reduced Yki activity, implying that Ing5 links the EGFR and Yki pathways (Fig. 7*L*).

First, we examined the expression of several Yki target genes using lacZ reporters and found a reduction of Yki activity in wing discs containing *Ing5-RNAi* tissues or *Ing5*-null clones. The reporter expression for *dMyc*, *ex*, *bantam*, and *CycE* was decreased in *en>Ing5-RNAi* wings (closed arrowheads in Fig. 3 *I* and *J* and *SI Appendix*, Fig. S4 *D* and *E*). *DIAP1-lacZ* expression was also moderately reduced in *Ing5*-null clones (*SI Appendix*, Fig. S4*F*). Next, we assessed whether the reduced wing size in *Ing5* mutants could be restored by increasing Yki activity through the genetic interaction between Ing5 and Hippo pathway components. Reducing Hpo, Wts, Mats, Ex, or Kibra activity in fly wings enhances Yki activity, thereby increasing wing size (Fig. 3*K*-#1–5) (72). Interestingly, the reduced wing size in *en>Ing5-RNAi* was restored by additional RNAi for *hpo*, *mats*, *kibra*, or *ex* (Fig. 3*K*-#8–12 and *SI Appendix*, Fig. S4*G*). Similarly, Yki overexpression in *en>Ing5-RNAi* wings restored wing size (Fig. 3*K*-#13–14). Increasing Yki activity in *en>Ing5-RNAi* wings also enhanced abnormal vein formation (Fig. 3*K*, white arrows), which is likely due to the ability of Yki to increase EGFR signaling activity (Fig. 3*H*) (70). Overall, these results suggest that the reduced wing size and ectopic wing veins in *Ing5* mutants may be caused by the dual functions of Ing5: positive regulation of Yki activity and negative regulation of EGFR signaling. The Ing5 function appears to be downstream of EGFR signaling and upstream of the Yki pathway. Additionally, based on the action of *Ing5* knockdown in suppressing wing size by EGFR overexpression (Fig. 3*A*-#10, black arrowhead), Ing5 may be required to maintain a functional balance between the EGFR and Yki pathways for optimal organ growth (Fig. 7*L*).

Ing5 Is Essential for the Suppression of Tissue Overgrowth and the Function of Enok. Our in vivo experiments showed that loss of Ing5 suppressed apoptosis in *rl*-knockdowned wings (*SI Appendix*, Fig. S4*C*). Additionally, the *Ing5* mutation increased EGFR signaling activity, though Yki activity was reduced in the same condition. The results suggest that the *Ing5* mutation may promote cell survival by affecting EGFR signaling.

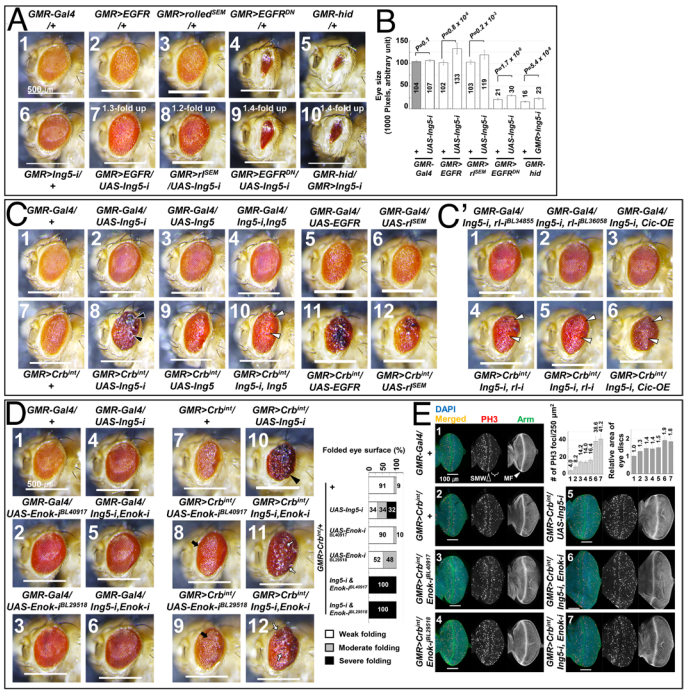

Fig. 4. Enhanced cell survival and tissue overgrowth by *Ing5* and *Enok* mutations. (*A* and *B*) Enhanced cell survival in eye tissues by Ing5 depletion. Additional *Ing5-RNAi* in *GMR>EGFR* and *GMR>rl*^{SEM} eyes (#2–3) increased eye size and roughness (#7–8). *Ing5-RNAi* suppressed apoptosis by EGFR signaling reduction (EGFR^{DN}) (#4, 9) or by Hid overexpression (#5, 10). (*B*) Quantitative analysis of panel *A*. n = 10 heads for each genotype. (*C* and *C'*) Enhanced *GMR>Crb*^{int} eye phenotypes by *Ing5-RNAi* and the EGFR pathway. (#1) *GMR-Gal4/+* control. (#7) *GMR–Gal4*-driven overexpression of the intracellular domain of Crumbs (*GMR>Crb*^{int}) caused eye roughness by Yki activity-induced overgrowth and cell survival. (#8, black arrowheads) *Ing5-RNAi* combined with *GMR>Crb*^{int} produced excessive roughness, melanization, and eye-surface folding, which were restored by additional Ing5 overexpression (#10, white arrowheads). (#11–12) Overexpressing EGFR or rl^{SEM} (an activated form of fly ERK) in *GMR>Crb*^{int} produced eye phenotypes similar to #8. (*C'*) Reduced EGFR signaling by *rl-RNAi* or *Cic* overexpression ameliorates *GMR>Crb*^{int}*/UAS-Ing5-RNAi* eye phenotypes (C-#8 and C'-#4–6). (*D* and *E*) Enhanced overgrowth in *GMR>Crb*^{int} eyes by *Ing5-Enok* double knockdown. (#1–6) In the absence of Crb^{int} overexpression, *GMR–Gal4*-driven single or double knockdown of *Ing5-RNAi* and *Enok-RNAi* formed no visible phenotype. (#7–9) *Enok* single knockdown in *GMR>Crb*^{int} eyes slightly increased eye size and roughness (black arrows) compared to *GMR>Crb*^{int}. (#10–12) *Ing5-Enok* double knockdown in *GMR>Crb*^{int} produces more severe eye phenotypes in size, roughness, and folding (#11–12, white arrows and histogram) compared to *Enok* single knockdown in *GMR>Crb*^{int} eyes (#8–9). (Histogram) Frequency of eye-surface folding in the presence of *GMR>Crb*^{int}. n = 79 flies for panel #7, 50 for #10, 73 for #8, 75 for #9, 51 for #11, and 54 for #12. (*E*) Increased cell proliferation and tissue size in *Ing5-Enok* double-knockdowned *GMR>Crb*^{int} larval eye discs. Adherens junction generally seems to be intact (Arm). Ten discs were used for quantification for each genotype.

In *Drosophila* eyes, EGFR signaling up-regulates the formation, differentiation, and survival of photoreceptors by inhibiting the expression of the proapoptotic protein Hid (73, 74). Thus, increased EGFR signaling in differentiating eyes by overexpressing EGFR or an activated form of ERK (*rl*^{SEM}) produced an excessive number of photoreceptors, resulting in a roughening of the adult eye (Fig. 4*A*-#1–3). In contrast, reduced EGFR signaling in *GMR>EGFR*^{DN} eyes induced Hid-dependent apoptosis, causing a severe reduction in eye size (Fig. 4*A*-#4–5) (75–79). Although *Ing5* knockdown itself did not affect eye phenotype compared to the wild type (Fig. 4*A*-#1 and #6), it significantly increased roughness and size (by 20 to 30%) in *GMR>EGFR* or *GMR>rl*^{SEM} eyes (Fig. 4 *A*-#7–8 and *B*). In addition, *Ing5* knockdown suppressed apoptosis in EGFR^{DN} or Hid-overexpression eyes (Fig. 4 *A*-#4, 5, 9, 10 and *B*). These results suggest that Ing5 depletion promotes cell survival by increasing EGFR signaling.

Next, we tested the genetic association between *Ing5* and Yki-related tissue overgrowth. Crumbs (Crb) is a transmembrane protein that acts upstream in the Hippo pathway as a tumor suppressor (80, 81). Misregulation of Crb induces an increase in Yki activity, thereby increasing organ/tissue size or promoting tumor formation (81–83). *GMR–Gal4*-driven overexpression of the intracellular domain of Crb (*GMR>Crb*^{int}) increased eye roughness due to the overgrowth of eye cells (Fig. 4 *C*-#1 and #7 and *E*-#1-2)

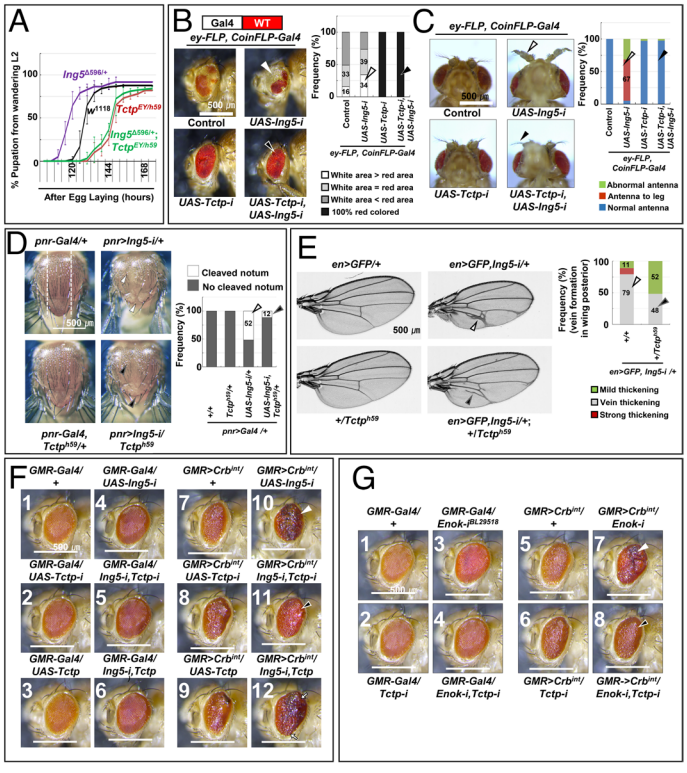

Fig. 5. Suppression of *Ing5/Enok* mutant phenotypes by additional *Tctp* mutation. (*A*) A strong hypomorphic *Tctp*$^{EY/h59}$ mutation suppressed the accelerated pupation of *Ing5Δ*^{596}/+ heterozygotes (*Ing5Δ*^{596}/+; *Tctp*$^{EY/h59}$, n = 120). *Ing5Δ*^{596}/+ heterozygotes (n = 62) pupated ~10 h earlier than *w*^{1118} controls (n = 200). *Tctp*$^{EY/h59}$ larvae show delayed pupal timing (n = 205). (*B* and *C*) *Ing5-RNAi* overexpression clones, produced by the *ey-FLP, CoinFLP-Gal4* method. (*B*) Gal4-overexpressing eye cells have no pigmentation. The *Ing5*-knockdown white area is often larger than the red-pigmented area (white arrowheads, 34% frequency, n = 38 heads). *Tctp-RNAi* addition suppresses this phenotype (black arrowheads, n = 33 heads). (*C*) Antenna-to-leg transformation of the *Ing5*-knockdowned clones in the antenna (white arrowheads, 67%, n = 38 heads) was completely restored by *Tctp-RNAi* addition (black arrowheads, n = 33 heads). (*D*) Thorax cleft of *pnr>Ing5-RNAi* animals (white arrowheads, 52%, n = 201 flies) was reduced by adding a *Tctp*^{h59}/+ allele (black arrowheads, n = 222). *pnr-Gal4* is expressed between two broken lines in the notum. (*E*) Abnormal vein formation in *en>Ing5-RNAi* wings (white arrowheads and histogram, n = 165 wings) was suppressed by introducing *Tctp*^{h59}/+ (black arrowheads and histogram, n = 197). (*F* and *G*) Tumor-like phenotypes in *Ing5-* or *Enok*-knockdowned *GMR>Crb*^{int} eyes (white arrowheads) were suppressed by additional *Tctp-RNAi* (black arrowheads). (*F*) (#1–6) *Ing5-RNAiTctp-RNAi*, Tctp overexpression, or their recombined expression using *GMR–Gal4* showed no abnormal phenotype. (#7–9) *GMR>Crb*^{int} eye phenotype was less affected by *Tctp-RNAi* addition and slightly enhanced by Tctp overexpression. (#10–12) Overgrowth in *Ing5*-knockdowned *GMR>Crb*^{int} eyes (white arrowhead) was suppressed by additional *Tctp-RNAi* (black arrowhead). Tctp overexpression moderately enhanced the Ing5-depleted *GMR>Crb*^{int} phenotype (arrow). (*G*) (#1–4) *GMR–Gal4-driven Enok-RNAiTctp-RNAi*, or *Enok-Tctp* double knockdown showed no abnormal phenotype. (#5–8) Mild overgrowth in Enok-depleted *GMR>Crb*^{int} eyes (white arrowhead) was strongly suppressed by *Tctp-RNAi* addition (black arrowhead).

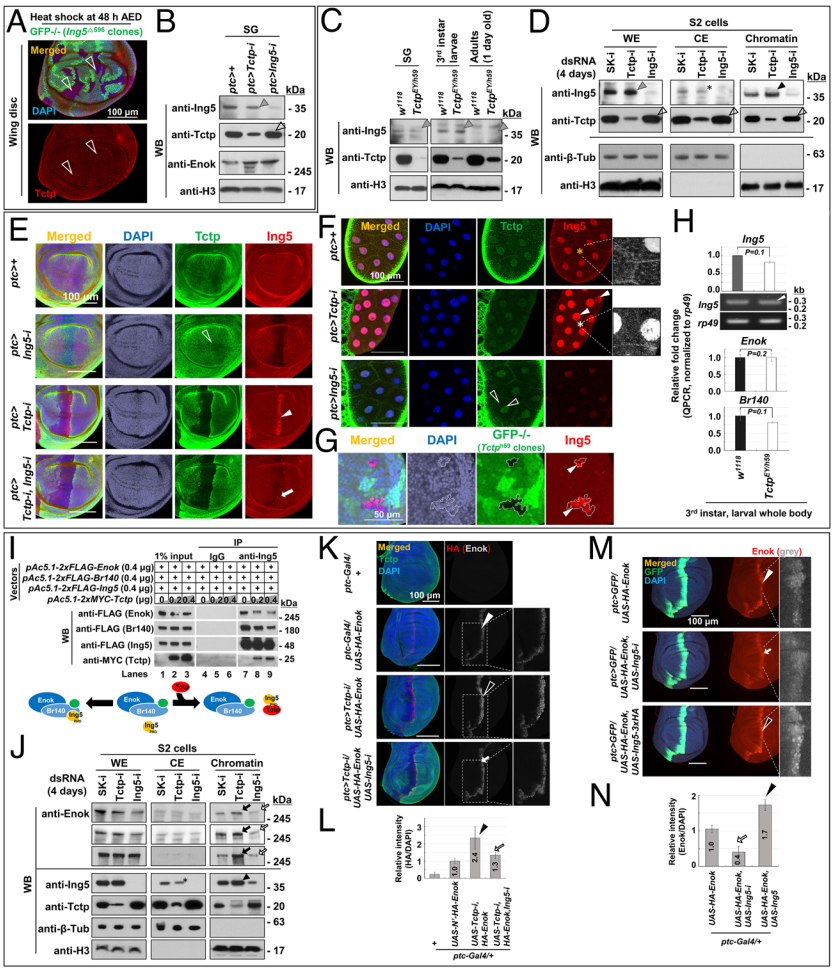

Fig. 6. Tctp inhibits Ing5 nuclear translocation and subsequent Enok binding to chromatin. (*A* and *B*) Intact Tctp protein level or subcellular localization in *Ing5* mutants (open arrowheads). (*A*) Intact Tctp level/distribution (red) in *Ing5*Δ^{596}-null clones (GFP-negative). (*B*) Tctp protein level was unaffected in *Ing5*-knockdowned SG tissues (open arrowhead) compared with *ptc-Gal4*/+ controls. Note intact Enok protein level in *Tctp*- or *Ing5*-knockdowned SGs. Histone H3 was the loading control for WB. (*C*–*H*) Induced nuclear translocation of Ing5 protein by *Tctp* reduction. (*C*) Intact Ing5 protein level in *Tctp*$^{EY/h59}$ strong hypomorphic mutants (gray arrowheads). Total protein extracts were obtained from larval SGs, larval bodies, or adult bodies. (*D*) In Tctp-knockdowned S2 cells, the total Ing5 protein level was intact (gray arrowhead) in WEs. However, Ing5 was highly accumulated in the chromatin fraction of cell extracts (black arrowhead) compared with *SK-RNAi*-treated controls. Notably, *Tctp* knockdown reduced the Ing5 level in the cytosolic fraction (CE, asterisk), suggesting nuclear translocation of Ing5. β-tubulin and histone H3 were quality controls for fractionation. (*E* and *F*) *Ptc>Tctp-RNAi* induces Ing5 nuclear accumulation in larval tissues (stained in red, filled arrowhead), which was specifically suppressed by *Ing5-RNAi* (arrow). Tctp level and distribution were unaffected by *Ing5-RNAi* (green, open arrowheads). Nuclei are stained in blue. (*F*) In SGs, Ing5 proteins in the cytosol appear in a mesh-like pattern (orange-colored asterisk and enlarged *Inset*). *Tctp* knockdown in SGs (*ptc>Tctp-RNAi*) increased Ing5 nuclear accumulation (white arrowheads) while decreasing cytosolic Ing5 levels (white asterisk and enlarged inset). (*G*) Ing5 nuclear accumulation (red, arrowheads) in wing discs containing *Tctp*^{h59}-null clones (GFP negative). (*H*) No changes in the *Ing5*, *Br140*, or *Enok* mRNA level in *Tctp*$^{EY/h59}$ larvae (quantitative PCR and white arrowhead in agarose gel electrophoresis). (*I*–*L*) Increased chromatin binding of Enok protein by Tctp reduction. (*I*) Co-IP using the anti-Ing5 antibody in S2 cell extracts expressing FLAG-tagged Enok, Br140, Ing5, and MYC-tagged Tctp. Ing5 formed a protein complex with Enok subunits (lane 7; middle to the left in the lower diagram), which was inhibited by Tctp protein in a concentration-dependent manner (lanes 8 and 9; middle to the right in the diagram). In the diagram, Tctp binding to the PHD motif of Ing5 was deduced from the in vitro pull-down results in Fig. 1. (*J*) In S2 cells, *Tctp* knockdown increased Enok levels in the chromatin fraction (black arrows), based on three independent experiments. Note a reduced level of chromatin-bound Enok by Ing5 knockdown (arrows). Enok bands in CE seem to be nonspecific. (*K* and *L*) Localization of HA-tagged Enok protein on chromatin (red, white arrowhead) is increased by ~2.4-fold by additional *Tctp-RNAi* (black arrowheads and histogram, n = 22 discs). The *Tctp-RNAi*-induced Enok chromatin enrichment was repressed by *Ing5-RNAi* (arrows and histogram, n = 12 discs). The box is enlarged in the *Right Inset*. (*M* and *N*) Ing5 regulates the binding of Enok to chromatin. Enok levels in chromatin/nuclei of *ptc>HA-tagged Enok* discs, stained using an anti-Enok antibody (red, white arrowhead), were reduced by additional *Ing5-RNAi* to 0.4-fold of the control value (arrows in *M* and *N*). In contrast, overexpression of HA-tagged Ing5 enhanced Enok nuclear levels by ~1.7-fold (black arrowheads in *M* and *N*). n = 10 discs for each genotype.

(81, 82, 84). Since the *Ing5* mutation reduced Yki activity and wing size in adults (Fig. 3 *I*, *J* and *SI Appendix*, Fig. S4 *D*, *E*, and *F*), we hypothesized that *Ing5* knockdown might suppress the rough eye phenotype in *GMR>Crb*^{int} flies. However, *Ing5* knockdown exacerbated the *GMR>Crb*^{int} phenotype, resulting in excessively roughened, melanized, and surface-folded eyes (Fig. 4*C*-#8). This synergistic enhancement by *Ing5* knockdown was specifically suppressed by additional Ing5 overexpression both in larval and adult eye tissues (*SI Appendix*, Fig. S5 and Fig. 4*C*-#10). Interestingly, the defective phenotype of *Ing5*-knockdowned *GMR>Crb*^{int} eyes was similar to that of EGFR- or rl^{SEM}-overexpressed *GMR>Crb*^{int} eyes (Fig. 4*C*-#11 and #12) and was also suppressed by the reduced EGFR activity by *rl-RNAi* or Cic overexpression (Fig. 4*C'*-#4–6). The results suggest that the *Ing5* mutation can promote tissue overgrowth combined with high or uncontrolled Yki activity by enhancing EGFR signaling.

Human ING5 forms different HAT complexes with an HBO1 or MOZ/MORF catalytic subunit (20), with the fly ortholog being Chameau (Chm) (85) or Enok (14, 15), respectively (*SI Appendix*, Fig. S6 *I* and *Q*). Unlike human ING5, fly *Ing5* only interacted with RNAi lines for Enok components (*SI Appendix*, Fig. S6 *O* and *P*) and affected Enok-mediated histone acetylation (*SI Appendix*, Fig. S6 *R* and *S*). Thus, we examined whether the Ing5-Enok HAT complex is also involved in the tissue overgrowth of *GMR>Crb*^{int} eyes. Although *Enok* single knockdown in *GMR>Crb*^{int} showed a mild increase in eye size, roughness, and folding of the eye surface (Fig. 4*D*-#8–9), *Enok-Ing5* double knockdown in *GMR>Crb*^{int} considerably increased eye size and folding (Fig. 4*D*-#11–12). Similar interactions were observed in larval eye discs (Fig. 4*E*). The results suggest that Ing5 is essential for Enok function and that the Ing5-Enok complex inhibits the tissue overgrowth produced by abnormally high Yki activity.

Phenotypes of *Ing5/Enok* Mutants Are Rescued by Additional *Tctp* Mutation. We examined the genetic interaction between *Ing5* and *Tctp* mutants to elucidate the physiological role of the direct binding between Tctp and Ing5. *Tctp* mutation causes defective tissue growth (38). However, additional *Ing5* knockdown in *en>Tctp* or *en>Tctp-RNAi* wings was additive (*SI Appendix*, Fig. S7 *A*, *Middle*) and not synergistic (*SI Appendix*, Fig. S7 *A*, *Bottom*). In contrast, *Tctp-RNAi* suppressed abnormal venation in *en>Ing5-RNAi* wings (*SI Appendix*, Fig. S7*A*, white and black arrowheads). Tctp overexpression exacerbated the abnormal venation in *en>Ing5-RNAi* wings (*SI Appendix*, Fig. S7*A*, orange arrowhead). This genetic antagonism on the *Ing5-RNAi* phenotype suggests that Tctp may be required to inhibit the Ing5 function in differentiation. Interestingly,

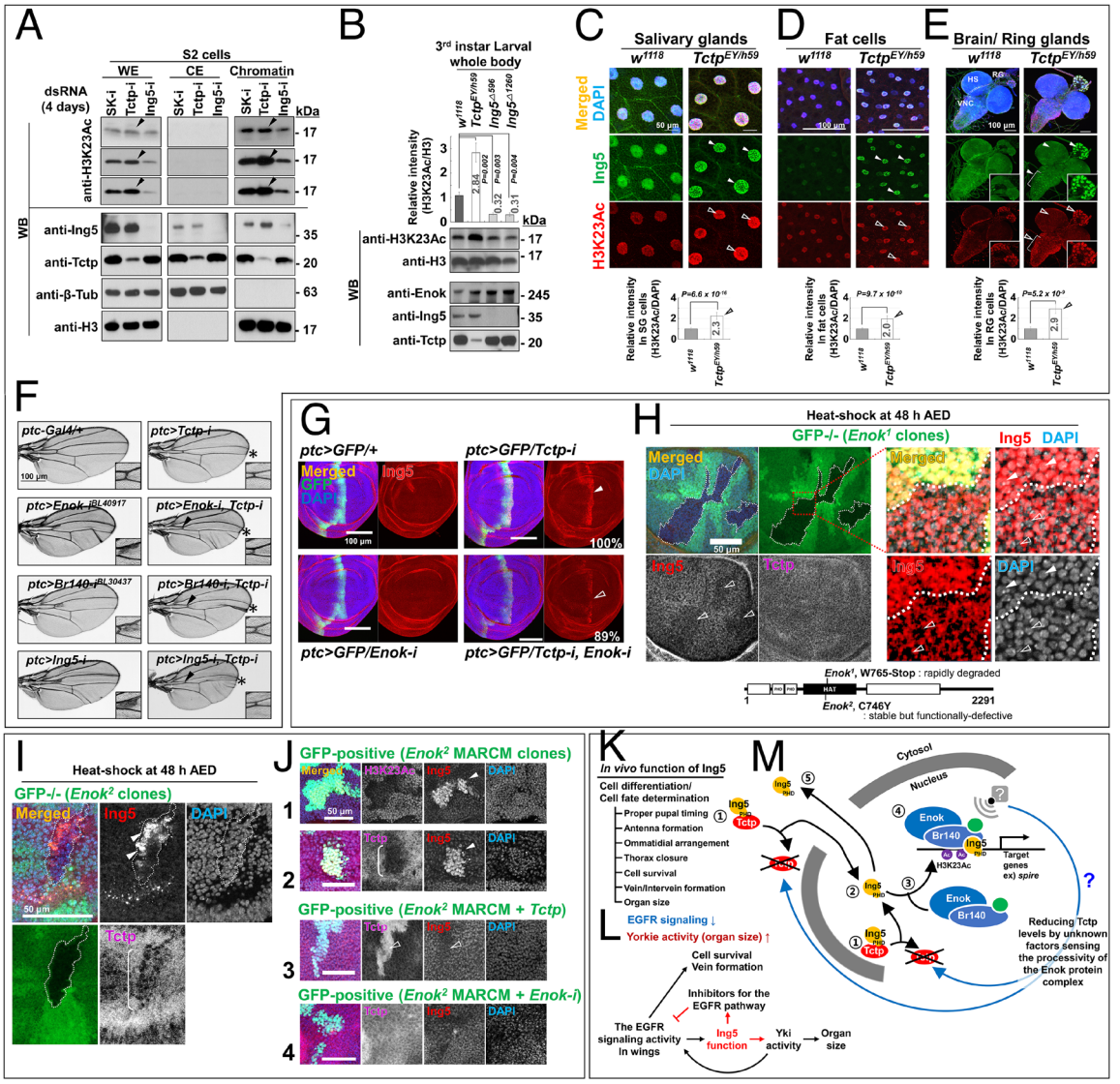

Fig. 7. Regulatory loop for maintaining the H3K23Ac level by Tctp, Ing5, and Enok. (*A*–*F*) Increased H3K23Ac level and Enok activity in *Tctp* mutants. (*A*) Tctp depletion using dsRNA in S2 cells increased H3K23Ac levels in WEs and chromatin (black arrowheads, performed three times independently). Histone H3 and β-tubulin were used as quality and loading controls for WB, respectively. (*B*) Increased H3K23Ac levels in $Tctp^{EY/h59}$ strong hypomorphic mutants. Decreased H3K23Ac levels in homozygous *Ing5* mutant larvae. A similar Enok protein level between *Tctp* and *Ing5* mutants is seen. Histone H3 was used as a loading control for WB. (*C*–*E*) Increased H3K23Ac levels (red) in cell nuclei from $Tctp^{EY/h59}$ larval tissues (open arrowheads), including SG cells, fat cells, brain hemispheres (HS), ventral nerve cord (VNC, brackets), and ring glands (RG, *Inset* images). Nuclear accumulation of Ing5 in $Tctp^{EY/h59}$ is also shown (stained in green, closed arrowheads). Histograms: quantified H3K23Ac levels in nuclei (n = 10 of SG, fat, or RG tissues) (*F*) Enhanced activity of the Enok complex by Tctp depletion rescues ACV thickening in *Enok-Br140-*, or *Ing5*-knockdowned wings (black arrowheads). *Insets*: enlarged ACV images. (Asterisks) Depleting Tctp decreased the distance between L3 and L4 veins. (*G* and *H*) Enok is required for the nuclear retention of Ing5. (*G*) Ing5 nuclear accumulation in *ptc>Tctp-RNAi* wing discs (closed arrowhead) was abolished by *Enok-RNAi* in 89% of the observed discs (open arrowhead). *Enok-RNAi* alone was insufficient in affecting Ing5 basal levels (*Bottom Left*). n = 20 discs for each genotype. (*H*) $Enok^{1}$-null clones in wing discs (GFP negative). A red-boxed area is enlarged on the right. Complete loss of *Enok* reduced the basal level of nuclear Ing5, or the nuclear retention of Ing5 (open arrowheads). Control clones (GFP positive) show a high level of nuclear Ing5 (closed arrowheads). Tctp protein level and subcellular distribution were unaffected in $Enok^{1}$-null clones. (*I* and *J*) A nonfunctional but stable form of Enok ($Enok^{2}$ allele) reduces Tctp level and provokes nuclear Ing5 translocation. Unlike the $Enok^{1}$ allele, $Enok^{2}$-null clones in wing discs (GFP-negative and -positive in panels *I* and *J*, respectively) produced a stable form of Enok protein without HAT activity (*J-1*). The MARCM method was used to overexpress *Tctp* (*J-3*) or *Enok-RNAi* (*J-4*) in $Enok^{2}$ clones. (*K*–*M*) Proposed model for the roles of Ing5-Enok-Tctp in *Drosophila*. Tctp inhibits ectopic H3K23Ac formation in chromatin for normal development. (*K*) In vivo, Ing5 is required for cell differentiation and fate determination in various developmental processes. (*L*) Dual functions of Ing5 in negative regulation of EGFR signaling and positive regulation of Yki activity. In our model, Ing5 is required for the expression of the inhibitory genes of EGFR signaling to regulate cell survival and venation. In addition, Ing5 links the EGFR pathway to the Yki pathway for organ size determination. Therefore, Ing5 reduction may be implicated in tumor formation when combined with uncontrolled Yki activity. (*M*) (1) Tctp binds to Ing5 to inhibit uncontrolled Ing5's nuclear translocation or binding to Enok. (2) Cytosolic Ing5 released from Tctp translocates into the cell nucleus, where free Ing5 binds the Enok complex and promotes chromatin association of Enok HAT (#2–4). (4) The Enok HAT complex acetylates H3K23. (5) Unbound nuclear Ing5 exits the nucleus. (Blue arrows with a question mark) Nonfunctional Enok protein induces a reduction in Tctp level (cross-marked Tctp) and subsequent accumulation of nuclear Ing5 to compensate for the reduced processivity of Enok and H3K23Ac levels. Factors controlling Tctp levels remain elusive.

this inhibitory effect was also observed at the epigenetic level. When chromatin structure was assayed using position effect variegation of the w^{m4+} allele (*SI Appendix*, Fig. S7*B*), an increase in chromatin compaction in the $Ing5\Delta^{596}$/+ mutation (*SI Appendix*, Fig. S7*B*, arrow) was significantly restored by additional $Tctp^{h59/+}$ mutation (*SI Appendix*, Fig. S7*B*, black arrowheads).

Next, we verified Tctp's inhibitory role in Ing5 function. Notably, the defective phenotypes of the *Ing5* mutants, including pupation timing, eye-antennal development, thorax cleft, wing vein formation, and tissue overgrowth under high Yki activity, were considerably suppressed by additional *Tctp* mutation: 1) The 10-h-accelerated pupal timing in $Ing5\Delta^{596/+}$ heterozygotes was masked by introducing

the *Tctp*$^{EY/h59}$ transheterozygous mutation (Fig. 5*A*). 2) The moderately increased area of *Ing5-RNAi* clones in adult eyes, generated by the CoinFLP method that produces Gal4-expressing mosaic clones in the eye-antennal discs (86), was also suppressed by additional *Tctp-RNAi* in the same cells (Fig. 5*B*, white and black arrowheads). 3) Moreover, the antenna-to-leg transformation of *Ing5-RNAi* clones in antenna discs was completely rescued by *Tctp-RNAi* addition in the same clones (Fig. 5*C*). 4) The thorax cleft observed in the *Ing5*-knockdowned notum (*pnr>Ing5-i*), as well as vein thickening in *en>Ing5-RNAi* wings, was rescued by reducing *Tctp* expression (Fig. 5 *D* and *E*). 5) Moreover, tissue overgrowth in *Ing5*- or *Enok*-knockdowned *GMR>crb*^{int} eyes was strongly suppressed by additional *Tctp* knockdown in both the adult and larval stages (Fig. 5 *F* and *G*, white and black arrowheads; *SI Appendix*, Fig. S7*C-#6* and *D-#5*). *Tctp* overexpression mildly enhanced the *Ing5*-knockdowned *GMR>Crb*^{int} overgrowth phenotype (Fig. 5*F*, arrows; *SI Appendix*, Fig. S7*C-#7*). These results suggest that Tctp is necessary to inhibit the activity of the Ing5 protein or Ing5-associated Enok complex in various physiological conditions.

Inhibitory Effects of Tctp on Ing5 Nuclear Translocation and Enok Chromatin Localization. The protein level and localization of Tctp in *Ing5*-knockdown or null mutants were intact (Fig. 6 *A* and *B* and *SI Appendix*, Fig. S8 *A* and *B*, open arrowheads). Thus, to elucidate the mechanisms by which Tctp negatively regulates the activity of Ing5, we assessed whether Tctp affects the amount or subcellular localization of Ing5 proteins. Western blot analyses of whole-cell extracts from *Tctp*-knockdowned SGs, wing discs, S2 cells, or *Tctp*$^{EY/h59}$ strong hypomorphic mutants showed no change in Ing5 protein levels (Fig. 6 *B–D* and *SI Appendix*, Fig. S8*B*, gray arrowheads). Instead, the distribution of Ing5 proteins increased in the chromatin of *Tctp*-knockdowned S2 cells but decreased in the cytosol (Fig. 6 *D* and *J*, black arrowhead and asterisk). A similar result was observed by IHC of *Tctp*-knockdowned SGs, where the mesh-like cytosolic Ing5 distribution disappeared and nuclear Ing5 levels increased (Fig. 6*F*, orange-/white-colored asterisks, and closed arrowheads). These results suggested that Tctp reduction induces nuclear translocation of Ing5.

IHC of larval tissues supported the chromatin accumulation of Ing5 by Tctp depletion. When *Tctp* was knocked down in the wings of *ptc>Tctp-i* larvae, Ing5 proteins were highly enriched in the cell nuclei (Fig. 6*E* and *SI Appendix*, Fig. S8*D*). Similar nuclear accumulation of Ing5 by Tctp depletion was observed in SGs from *Tctp*$^{EY/h59}$ mutants and wing discs with *Tctp*-null clones (Fig. 6*G* and *SI Appendix*, Fig. S8*C*) or *en>Tctp-RNAi* tissues (*SI Appendix*, Fig. S8*A*). The nuclear accumulation of Ing5 in *ptc>Tctp-RNAi* wing discs was specifically abolished by additional *Ing5-RNAi* (Fig. 6*E*, arrow). Notably, the nuclear accumulation of Ing5 in *Tctp*$^{EY/h59}$ mutants was not due to the increased gene expression of *Ing5*, *Enok*, or *Br140*, according to quantitative PCR (Fig. 6*H*).

We assessed whether Tctp also regulates the chromatin localization of Enok. First, we examined whether Tctp interferes with the formation of Ing5-Enok complexes. A co-IP assay using an Ing5 antibody and S2 cell extracts expressing Flag-tagged Enok subunits (Enok, Ing5, or Br140) showed that MYC-tagged Tctp decreased the level of interaction between Ing5 and Enok subunits in a concentration-dependent manner (Fig. 6*I*, lanes 7, 8, and 9; lower diagrams), which suggests that the binding of Tctp to Ing5 competitively inhibits the interaction between Ing5 and Enok, which inhibits the localization of Enok to chromatin.

Indeed, *Tctp*-knockdown S2 cells showed enriched Enok levels in the chromatin (Fig. 6*J*, black arrows), indicating that Tctp depletion facilitates the formation of the Ing5-Enok complex and its localization to chromatin. Both IHC of larval wings and genetic analysis of adult wings confirmed this enrichment of Enok on chromatin by Tctp depletion. In wing discs, we observed overexpressed HA-tagged Enok (*ptc>N'-HA-Enok*) in the cell nuclei (Fig. 6*K*, white arrowhead). Additional *Tctp-RNAi* enhanced the nuclear accumulation of Enok by ~2.4-fold (Fig. 6 *K* and *L*, black arrowheads). Genetic interaction between overexpressed *HA-Enok* and *Tctp-RNAi* confirmed this outcome: The phenotype with no anterior-crossvein (ACV) observed in ~74% of *ptc>N'-HA-Enok* wings was enhanced to 100% by additional Tctp depletion (*SI Appendix*, Fig. S8*E*).

Finally, we showed that Ing5 was essential for the chromatin binding of Enok in vivo. In S2 cells, the Enok protein level in the chromatin fraction was considerably reduced by Ing5 depletion (Fig. 6*J*, white arrows). Additionally, the chromatin binding of Enok in *ptc>N'-HA-Enok* larval wings was significantly suppressed by *Ing5-RNAi* (Fig. 6 *M* and *N*, white arrowhead and arrow) while being enhanced by Ing5 overexpression (Fig. 6 *M* and *N*, black arrowheads). *Tctp-RNAi*-enhanced Enok accumulation on chromatin was also reduced by additional *Ing5-RNAi* (Fig. 6 *K* and *L*, black arrowheads and white arrows). Genetic interaction between Enok and Ing5 confirmed the chromatin localization of Enok controlled by Ing5: We found that the 78% penetrance of no ACV phenotype in *ptc>N'-HA-Enok* wings was reduced to 25% by Ing5 depletion (*SI Appendix*, Fig. S8*F*, open arrowhead) and enhanced to 100% by Ing5 overexpression (*SI Appendix*, Fig. S8*F*, black arrowhead).

Collectively, our results demonstrate that the binding of Tctp to Ing5 negatively regulates the chromatin binding of Enok by inhibiting the nuclear translocation of Ing5 and subsequent complex formation with Enok.

Regulatory Loop to Maintain Proper H3K23Ac Levels between Tctp, Ing5, and Enok. We found that the in vivo depletion of Tctp promotes the chromatin accumulation of Ing5 and Enok proteins. The *Drosophila* Enok HAT complex acetylates histone H3 at lysine 23 (H3K23Ac) (*SI Appendix*, Figs. S6 *R* and *S* and S9 *I–K*) (14, 15). Therefore, we assessed whether the global level of H3K23Ac is up-regulated by the chromatin accumulation of Ing5 and Enok in *Tctp* mutants. First, we found an increase in the H3K23Ac level in Tctp-depleted S2 cells. Consistent with the chromatin binding of Ing5 and Enok by Tctp depletion (Figs. 6 *D–L* and 7*A*), the H3K23Ac level increased in both whole-cell and chromatin extracts from Tctp-depleted S2 cells compared to *SK-i* controls (Fig. 7*A*, black arrowheads). Second, the H3K23Ac level of third-instar *Tctp*$^{EY/h59}$ mutant larvae also increased by ~2.8-fold compared to wild-type controls (Fig. 7*B*). Third, we observed a twofold-to-threefold-increase in the H3K23Ac level in *Tctp*$^{EY/h59}$ tissues (Fig. 7 *C–E*, red and histogram) with simultaneously high nuclear Ing5 levels (Fig. 7 *C–E*, green). Lastly, the complete rescue of the ACV thickening in *Enok*-, *Br140*-, or *Ing5*-knockdowned wings by *Tctp-RNAi* addition (Fig. 7*F*) suggested an increase in Enok HAT activity by Tctp depletion. Collectively, our experiments with S2 cells and fly tissues indicate that Tctp negatively regulates H3K23Ac by inhibiting chromatin binding of the Ing5-Enok HAT complex.

Finally, we assessed whether Enok affects the subcellular localization of Ing5 or Tctp. When *Enok-RNAi* was coexpressed in *ptc>Tctp-RNAi* discs (which showed 100% penetrance of Ing5-chromatin accumulation) (Fig. 7*G*), about 89% of wing discs with *Tctp-Enok* double knockdown showed reduced accumulation of nuclear Ing5 (Fig. 7*G*), indicating that Enok may be required for its nuclear retention. We analyzed the role of Enok in the nuclear retention of Ing5 using a LOF *Enok*^{1} mutation. The *Enok*^{1} allele is functionally null and produces a rapidly degradable truncated protein without HAT activity due to a nonsense mutation in the HAT domain (*SI Appendix*, Fig. S10 *A* and *B*) (14). Larval wings containing *Enok*^{1}-null clones showed a moderate but

obvious reduction in the nuclear level of Ing5 protein compared with surrounding cells (Fig. 7*H*, open and closed arrowheads). The Tctp protein level and its subcellular localization were unaffected in *Enok*^{1}-mutant clones (Fig. 7*H*).

An interesting and unexpected result was observed in *Enok*^{2}-null clones. The *Enok*^{2} allele produces stable but nonfunctional HAT proteins with a missense mutation in the HAT domain (*SI Appendix*, Fig. S10 *A* and *C*) (14). Unlike the *Enok*^{1} clones, wing discs bearing the *Enok*^{2}-null clones showed a high accumulation of nuclear Ing5 and low level of Tctp (Fig. 7 *I*, J-#1–2, closed arrowheads and bracket), which was suppressed in *Enok*^{2} clones overexpressing Tctp in the same cells (Fig. 7*J*-#3). Additional *Enok* knockdown in *Enok*^{2} clones attenuated both Tctp reduction and Ing5 accumulation (Fig. 7*J*-#4), similar to the result for *Enok*^{1}-null clones. These results suggest that, in *Enok*^{1} clones, nuclear Ing5 may not be maintained efficiently due to the lack of Enok protein; however, in *Enok*^{2} clones, inactive Enok^{2} protein may form a stable complex with nuclear Ing5 while reducing Tctp levels. Moreover, our results point to the existence of a dynamic feedback loop between Tctp, Ing5, and Enok maintaining the global H3K23Ac level at appropriate levels. First, Tctp down-regulates the chromatin binding of Enok and ectopic H3K23Ac formation by inhibiting the nuclear translocation of Ing5. Second, the lack of Enok processivity promotes the nuclear localization of Ing5 to enhance the activity and chromatin localization of the Enok complex by reducing Tctp levels (Fig. 7*M*).

Discussion

This study was initiated following the discovery of physical interaction between Tctp and Ing5. A key question is how the interaction regulates the function of the Enok HAT complex, including histone acetylation in chromatin modification. The functions of MOZ/MORF/Enok have been studied extensively in mice, *Drosophila*, and human cell lines (2, 29). However, the mechanism/protein by which the localization of ING5 and MOZ/MORF/Enok complex is controlled is still poorly understood. Human ING5 is required for MOZ function in HeLa cells (20); however, whether dynamic changes in ING5 localization, such as nuclear translocation, regulate the binding of MOZ/MORF to chromatin in vitro or in vivo have not yet been addressed. In addition, although the involvement of MOZ/MORF/ING5 in tumorigenesis is well characterized, their interaction with other signaling pathways has been less studied in vivo (29).

Here, we used *Drosophila* as a model and showed that Tctp is an important negative regulator of the nuclear translocation of Ing5 and that Ing5 is essential for the binding of Enok to chromatin in regulating global H3K23Ac levels. The inhibitory effect of Tctp on Enok/Ing5-mediated histone acetylation demonstrates that Tctp functions as a safeguard against uncontrolled gene expression at the global level. We also observed a feedback mechanism between Tctp, Ing5, and Enok that compensates for the reduced processivity of Enok HAT by actively controlling Tctp levels and Ing5 localization. Our analysis of *Drosophila Ing5* mutants provides an animal study to elucidate the in vivo function of the *Ing5* gene. In *Drosophila*, the functions of the Enok complex have mainly been studied in larval neurons, ovaries, and early embryos (11, 13, 15, 17, 18). However, its function in other somatic tissues or the adult stage has been unexplored. Using *Ing5*-null mutants, we demonstrate that the Enok complex plays multiple roles in late developmental processes of body formation, such as homeotic transformation, thorax closure, and organ size determination, previously unidentified phenotypes. The defective phenotypes of adult flies with *Ing5* mutation have features common with those of human patients with developmental disorders, including DiGeorge syndrome. Therefore, our study on fly Tctp–Ing5–Enok interaction may provide mechanistic insights into various human diseases associated with MOZ/MORF/ING5. Furthermore, fly *Ing5* mutants may be useful disease models for studying MOZ/MORF/ING5-related human diseases.

Consistent with its role in the global acetylation of H3K23, Ing5 depletion produced various phenotypes in developing flies. As summarized in Fig. 7 *K*–*M*, Ing5 participates in various developmental processes by mainly controlling cellular differentiation rather than cell proliferation (Fig. 7*K*). Ing5 interacts with at least two signaling pathways, negatively regulating EGFR signaling to control wing development and cell survival and positively regulating the Yki pathway to regulate organ size (Fig. 7*L*). We showed that the loss of Ing5 alone does not cause overgrowth in developing tissues; however, the combined loss of Ing5 and Enok is critical for suppressing tissue overgrowth when Yki signaling is strongly activated by Crb misregulation. This suggests that Ing5 and Enok may be required for tumor suppression in specific conditions, such as Yki-related tumor formation, and that their roles in differentiation are important for suppressing tumorigenesis.

Based on our findings, we propose that Tctp maintains normal developmental processes by negatively regulating ectopic Enok/Ing5 complex activity for H3K23 acetylation (Fig. 7*M*). In *Drosophila*, Tctp and Ing5 regulate Enok-dependent gene regulation through the following process: 1) Tctp anchors Ing5 in the cytosol by direct interaction and inhibits the binding of Ing5 with Enok catalytic subunits in the cell nucleus. Given that Ing5 and Tctp coexist in the cytosol and nucleus, Tctp may also inhibit Ing5 activity in the cell nucleus. 2) Tctp depletion causes Ing5 to be released and translocated to the nucleus. 3 and 4) Nuclear Ing5 forms a protein complex with other Enok subunits and binds to chromatin. The Enok/Ing5 complex activates the H3K23Ac modification on chromatin to regulate the expression of various target genes. 5) Based on the depletion of Ing5 in *Enok*-mutated tissues (Fig. 7 *G* and *H*, J-#4), an unbound form of Ing5 may exit the cell nucleus. It remains unknown how the dissociating process between Ing5 and Tctp is regulated (Fig. 7*M*, blue-colored arrows with a question mark). We postulate that a similar mechanism exists in humans since we glanced at the inhibitory role of TCTP on ING5 nuclear accumulation in SCC25 human cell lines (*SI Appendix*, Fig. S11). However, further studies are required to confirm this clearly.

Materials and Methods

Methods and information for *Drosophila* culture, human cell culture, protein–protein interaction, immunostaining, western blotting, antibodies, and PCR are given in *SI Appendix, SI Materials and Methods*. For statistical analysis, data were analyzed using a *t* test in Excel (Microsoft). Data are expressed as mean ± SD.

Data, Materials, and Software Availability. All study data are included in the article and/or *SI Appendix*.

ACKNOWLEDGMENTS. We thank Fu Huang, Jessica Treisman, Elisabeth Knust, Takashi Suzuki, and Kyung-Ok Cho for their aid, advice, and reagents. We acknowledge the assistance of the Korea *Drosophila* Resource Center, Bloomington *Drosophila* Stock Center, National Institute of Genetics Stock Center, Vienna *Drosophila* Resource Center, *Drosophila* Genomics Resource Center, and Developmental Studies Hybridoma Bank in providing fly stocks or antibodies. This work was supported by grants from the National Research Foundation of Korea funded by the Korea government (Ministry of Education or Ministry of Science and ICT; NRF-2016R1D1A1B03932093 and NRF-2020R1A2C2006664 to S-T.H.; NRF-2014K1A1A2042982 and NRF-2017R1A2B3007516 to K.-W.C; NRF-2022R1A6A3A01087289 to L.-H.K.; NRF-2021R1C1C1014142 and Chungnam National University Hospital Research Fund, 2022 to J.W.C.).

Author affiliations: [a]Department of Anatomy and Cell Biology, College of Medicine, Chungnam National University, Daejeon 35015, Republic of Korea; [b]Department of Medical Science, College of Medicine, Chungnam National University, Daejeon 35015, Republic of Korea; [c]Department of Otolaryngology-Head and Neck Surgery, College of Medicine, Chungnam National University, Daejeon 35015, Republic of Korea; [d]Korea Drosophila Resource Center, Gwangju Institute of Science and Technology, Gwangju 61005, Republic of Korea; [e]School of Life Sciences, Gwangju Institute of Science and Technology, Gwangju 61005, Republic of Korea; and [f]Department of Biological Sciences, Korea Advanced Institute of Science & Technology, Daejeon 34141, Republic of Korea

Author contributions: S.-T.H. designed research; L.-H.K., J.-Y.K., Y.-Y.X., and M.A.L. performed research; B.S.K., J.H.K., S.-E.Y., and Y.-J.K. contributed new reagents/analytic tools; Y.-Y.X. analyzed data; and L.-H.K., J.-Y.K., K.-W.C., J.W.C., and S.-T.H. wrote the paper.

1. E. R. Gibney, C. M. Nolan, Epigenetics and gene expression. *Heredity (Edinb)* **105**, 4–13 (2010).
2. F. Huang, S. M. Abmayr, J. L. Workman, Regulation of KAT6 acetyltransferases and their roles in cell cycle progression, stem cell maintenance, and human disease. *Mol. Cell Biol.* **36**, 1900–1907 (2016).
3. X. J. Yang, MOZ and MORF acetyltransferases: Molecular interaction, animal development and human disease. *Biochim. Biophys. Acta Mol. Cell Res.* **1853**, 1818–1826 (2015).
4. S. Rokudai *et al.*, MOZ increases p53 acetylation and premature senescence through its complex formation with PML. *Proc. Natl. Acad. Sci. U.S.A.* **110**, 3895–3900 (2013).
5. B. N. Sheikh *et al.*, MOZ (MYST3, KAT6A) inhibits senescence via the INK4A-ARF pathway. *Oncogene* **34**, 5807–5820 (2015).
6. F. M. Perez-Campo *et al.*, MOZ-mediated repression of p16(INK4a) is critical for the self-renewal of neural and hematopoietic stem cells. *Stem Cells* **32**, 1591–1601 (2014).
7. T. Katsumoto *et al.*, MOZ is essential for maintenance of hematopoietic stem cells. *Genes Dev.* **20**, 1321–1330 (2006).
8. B. N. Sheikh *et al.*, MOZ and BMI1 play opposing roles during Hox gene activation in ES cells and in body segment identity specification in vivo. *Proc. Natl. Acad. Sci. U.S.A.* **112**, 5437–5442 (2015).
9. N. Pelletier, N. Champagne, S. Stifani, X. J. Yang, MOZ and MORF histone acetyltransferases interact with the Runt-domain transcription factor Runx2. *Oncogene* **21**, 2729–2740 (2002).
10. B. J. Klein, M. E. Lalonde, J. Cote, X. J. Yang, T. G. Kutateladze, Crosstalk between epigenetic readers regulates the MOZ/MORF HAT complexes. *Epigenetics* **9**, 186–193 (2014).
11. E. K. Scott, T. Lee, L. Luo, enok encodes a Drosophila putative histone acetyltransferase required for mushroom body neuroblast proliferation. *Curr. Biol.* **11**, 99–104 (2001).
12. J. Berger *et al.*, Systematic identification of genes that regulate neuronal wiring in the Drosophila visual system. *PLoS Genet.* **4**, e1000085 (2008).
13. T. Xin *et al.*, The Drosophila putative histone acetyltransferase Enok maintains female germline stem cells through regulating Bruno and the niche. *Dev. Biol.* **384**, 1–12 (2013).
14. F. Huang *et al.*, Histone acetyltransferase Enok regulates oocyte polarization by promoting expression of the actin nucleation factor spire. *Genes Dev.* **28**, 2750–2763 (2014).
15. F. Huang *et al.*, The Enok acetyltransferase complex interacts with Elg1 and negatively regulates PCNA unloading to promote the G1/S transition. *Genes Dev.* **30**, 1198–1210 (2016).
16. Z. Umer *et al.*, Genome-wide RNAi screen in Drosophila reveals Enok as a novel trithorax group regulator. *Epigenetics Chromatin* **12**, 55 (2019).
17. H. Kang *et al.*, Bivalent complexes of PRC1 with orthologs of BRD4 and MOZ/MORF target developmental genes in Drosophila. *Genes Dev.* **31**, 1988–2002 (2017).
18. S. Y. Tsai, F. Huang, Acetyltransferase Enok regulates transposon silencing and piRNA cluster transcription. *PLoS Genet.* **17**, e1009349 (2021).
19. M. Ullah *et al.*, Molecular architecture of quartet MOZ/MORF histone acetyltransferase complexes. *Mol. Cell Biol.* **28**, 6828–6843 (2008).
20. Y. Doyon *et al.*, ING tumor suppressor proteins are critical regulators of chromatin acetylation required for genome expression and perpetuation. *Mol. Cell* **21**, 51–64 (2006).
21. A. Dantas *et al.*, Biological functions of the ING proteins. *Cancers (Basel)* **11**, 1817 (2019).
22. R. Zhang, J. Jin, J. Shi, Y. Hou, INGs are potential drug targets for cancer. *J. Cancer Res. Clin. Oncol.* **143**, 189–197 (2017).
23. B. Cengiz *et al.*, Tumor-specific mutation and downregulation of ING5 detected in oral squamous cell carcinoma. *Int. J. Cancer* **127**, 2088–2094 (2010).
24. X. Li *et al.*, Decreased nuclear expression and increased cytoplasmic expression of ING5 may be linked to tumorigenesis and progression in human head and neck squamous cell carcinoma. *J. Cancer Res. Clin. Oncol.* **136**, 1573–1583 (2010).
25. H. C. Zheng, P. Xia, X. Y. Xu, H. Takahashi, Y. Takano, The nuclear to cytoplasmic shift of ING5 protein during colorectal carcinogenesis with their distinct links to pathologic behaviors of carcinomas. *Hum. Pathol.* **42**, 424–433 (2011).
26. F. Wang *et al.*, ING5 activity in self-renewal of glioblastoma stem cells via calcium and follicle stimulating hormone pathways. *Oncogene* **37**, 286–301 (2018).
27. G. Ormaza *et al.*, The tumor suppressor ING5 is a dimeric, bivalent recognition molecule of the histone H3K4me3 mark. *J. Mol. Biol.* **431**, 2298–2319 (2019).
28. M. Shiseki *et al.*, p29ING4 and p28ING5 bind to p53 and p300, and enhance p53 activity. *Cancer Res.* **63**, 2373–2378 (2003).
29. N. Wiesel-Motiuk, Y. G. Assaraf, The key roles of the lysine acetyltransferases KAT6A and KAT6B in physiology and pathology. *Drug Resist. Updat.* **53**, 100729 (2020).
30. W. Xie *et al.*, Tripartite motif containing 24 regulates cell proliferation in colorectal cancer through YAP signaling. *Cancer Med.* **9**, 6367–6376 (2020).
31. M. Kraft *et al.*, Disruption of the histone acetyltransferase MYST4 leads to a Noonan syndrome-like phenotype and hyperactivated MAPK signaling in humans and mice. *J. Clin. Invest.* **121**, 3479–3491 (2011).
32. U. Linzen *et al.*, ING5 is phosphorylated by CDK2 and controls cell proliferation independently of p53. *PLoS One* **10**, e0123736 (2015).
33. K. W. Mulder *et al.*, Diverse epigenetic strategies interact to control epidermal differentiation. *Nat. Cell Biol.* **14**, 753–763 (2012).
34. U. A. Bommer, A. Telerman, Dysregulation of TCTP in biological processes and diseases. *Cells* **9**, 1632 (2020).
35. R. Amson, S. Pece, J. C. Marine, P. P. Di Fiore, A. Telerman, TPT1/ TCTP-regulated pathways in phenotypic reprogramming. *Trends Cell Biol.* **23**, 37–46 (2013).
36. A. Telerman, R. Amson, The molecular programme of tumour reversion: The steps beyond malignant transformation. *Nat. Rev. Cancer* **9**, 206–216 (2009).
37. F. Brioudes, A. M. Thierry, P. Chambrier, B. Mollereau, M. Bendahmane, Translationally controlled tumor protein is a conserved mitotic growth integrator in animals and plants. *Proc. Natl. Acad. Sci. U.S.A.* **107**, 16384–16389 (2010).
38. Y. C. Hsu, J. J. Chern, Y. Cai, M. Liu, K. W. Choi, Drosophila TCTP is essential for growth and proliferation through regulation of dRheb GTPase. *Nature* **445**, 785–788 (2007).
39. T. P. Le, L. T. Vuong, A. R. Kim, Y. C. Hsu, K. W. Choi, 14-3-3 proteins regulate Tctp-Rheb interaction for organ growth in Drosophila. *Nat. Commun.* **7**, 11501 (2016).
40. R. Amson *et al.*, Reciprocal repression between P53 and TCTP. *Nat. Med* **18**, 91–99 (2012).
41. A. Burgess *et al.*, Chfr interacts and colocalizes with TCTP to the mitotic spindle. *Oncogene* **27**, 5554–5566 (2008).
42. F. Li, D. Zhang, K. Fujise, Characterization of fortilin, a novel antiapoptotic protein. *J. Biol. Chem.* **276**, 47542–47549 (2001).
43. L. Susini *et al.*, TCTP protects from apoptotic cell death by antagonizing bax function. *Cell Death Differ.* **15**, 1211–1220 (2008).
44. C. Cans *et al.*, Translationally controlled tumor protein acts as a guanine nucleotide dissociation inhibitor on the translation elongation factor eEF1A. *Proc. Natl. Acad. Sci. U.S.A.* **100**, 13892–13897 (2003).
45. J. Zhang *et al.*, Role of the translationally controlled tumor protein in DNA damage sensing and repair. *Proc. Natl. Acad. Sci. U.S.A.* **109**, E926–E933 (2012).
46. S. T. Hong, K. W. Choi, TCTP directly regulates ATM activity to control genome stability and organ development in Drosophila melanogaster. *Nat. Commun.* **4**, 2986 (2013).
47. S. R. Lee, S. T. Hong, K. W. Choi, Regulation of epithelial integrity and organ growth by Tctp and coracle in Drosophila. *PLoS Genet.* **16**, e1008885 (2020).
48. J. Jung, S. Ryu, I. A. Ki, H. A. Woo, K. Lee, Some biological consequences of the inhibition of Na, K-ATPase by translationally controlled tumor protein (TCTP). *Int. J. Mol. Sci.* **19**, 1657 (2018).
49. S. M. MacDonald, T. Rafnar, J. Langdon, L. M. Lichtenstein, Molecular identification of an IgE-dependent histamine-releasing factor. *Science* **269**, 688–690 (1995).
50. M. Tuynder *et al.*, Biological models and genes of tumor reversion: Cellular reprogramming through tpt1/TCTP and SIAH-1. *Proc. Natl. Acad. Sci. U.S.A.* **99**, 14976–14981 (2002).
51. S. Nam, T. P. Le, S. Chung, K. W. Choi, Tctp regulates the level and localization of Foxo for cell growth in Drosophila. *Cell Death Discov.* **8**, 146 (2022).
52. D. W. Yang *et al.*, Topoisomerase II is regulated by translationally controlled tumor protein for cell survival during organ growth in Drosophila. *Cell Death Dis.* **12**, 811 (2021).
53. Y. V. Kwon *et al.*, The role of translationally controlled tumor protein in proliferation of Drosophila intestinal stem cells. *Proc. Natl. Acad. Sci. U.S.A.* **116**, 26591–26598 (2019), 10.1073/pnas.1910850116.
54. S. T. Hong, K. W. Choi, Antagonistic roles of Drosophila Tctp and Brahma in chromatin remodelling and stabilizing repeated sequences. *Nat. Commun.* **7**, 12988 (2016).
55. A. H. Brand, N. Perrimon, Targeted gene expression as a means of altering cell fates and generating dominant phenotypes. *Development* **118**, 401–415 (1993).
56. N. A. Theodosiou, T. Xu, Use of FLP/FRT system to study Drosophila development. *Methods* **14**, 355–365 (1998).
57. D. J. Andrew, K. D. Henderson, P. Seshaiah, Salivary gland development in Drosophila melanogaster. *Mech Dev.* **92**, 5–17 (2000).
58. R. S. Stowers, T. L. Schwarz, A genetic method for generating Drosophila eyes composed exclusively of mitotic clones of a single genotype. *Genetics* **152**, 1631–1639 (1999).
59. S. S. Blair, Wing vein patterning in Drosophila and the analysis of intercellular signaling. *Annu. Rev. Cell Dev. Biol.* **23**, 293–319 (2007).
60. J. Y. Roignant, S. Hamel, F. Janody, J. E. Treisman, The novel SAM domain protein aveugle is required for Raf activation in the Drosophila EGF receptor signaling pathway. *Gene Dev.* **20**, 795–806 (2006).
61. M. Malartre, Regulatory mechanisms of EGFR signalling during Drosophila eye development. *Cell Mol. Life Sci.* **73**, 1825–1843 (2016).
62. M. Angulo, M. Corominas, F. Serras, Activation and repression activities of ash2 in Drosophila wing imaginal discs. *Development* **131**, 4943–4953 (2004).
63. F. Roch, G. Jimenez, J. Casanova, EGFR signalling inhibits Capicua-dependent repression during specification of Drosophila wing veins. *Development* **129**, 993–1002 (2002).
64. D. Brentrup, H. Lerch, H. Jackle, M. Noll, Regulation of Drosophila wing vein patterning: Net encodes a bHLH protein repressing rhomboid and is repressed by rhomboid-dependent Egfr signalling. *Development* **127**, 4729–4741 (2000).
65. A. S. Tseng *et al.*, Capicua regulates cell proliferation downstream of the receptor tyrosine kinase/ras signaling pathway. *Curr. Biol.* **17**, 728–733 (2007).
66. S. Y. Kim *et al.*, Negative regulation of EGFR/MAPK pathway by Pumilio in Drosophila melanogaster. *PLoS One* **7**, e34016 (2012).
67. L. K. MacDougall, M. E. Gagou, S. J. Leevers, E. Hafen, M. D. Waterfield, Targeted expression of the class II phosphoinositide 3-kinase in Drosophila melanogaster reveals lipid kinase-dependent effects on patterning and interactions with receptor signaling pathways. *Mol. Cell Biol.* **24**, 796–808 (2004).
68. R. D. Read, W. K. Cavenee, F. B. Furnari, J. B. Thomas, A drosophila model for EGFR-Ras and PI3K-dependent human glioma. *PLoS Genet.* **5**, e1000374 (2009).
69. Y. Jin *et al.*, EGFR/Ras signaling controls Drosophila intestinal stem cell proliferation via capicua-regulated genes. *PLoS Genet.* **11**, e1005634 (2015).
70. H. Herranz, X. Hong, S. M. Cohen, Mutual repression by bantam miRNA and Capicua links the EGFR/MAPK and Hippo pathways in growth control. *Curr. Biol.* **22**, 651–657 (2012).
71. H. Herranz, X. Hong, N. T. Hung, P. M. Voorhoeve, S. M. Cohen, Oncogenic cooperation between SOCS family proteins and EGFR identified using a Drosophila epithelial transformation model. *Gene Dev.* **26**, 1602–1611 (2012).
72. S. Sun, K. D. Irvine, Cellular organization and cytoskeletal regulation of the Hippo signaling network. *Trends Cell Biol.* **26**, 694–704 (2016).
73. A. Bergmann, J. Agapite, K. McCall, H. Steller, The Drosophila gene hid is a direct molecular target of Ras-dependent survival signaling. *Cell* **95**, 331–341 (1998).
74. M. Freeman, Reiterative use of the EGF receptor triggers differentiation of all cell types in the Drosophila eye. *Cell* **87**, 651–660 (1996).

75. W. H. Biggs III, *et al.*, The Drosophila rolled locus encodes a MAP kinase required in the sevenless signal transduction pathway. *EMBO J.* **13**, 1628–1635 (1994).
76. A. B. Corl *et al.*, Happyhour, a Ste20 family kinase, implicates EGFR signaling in ethanol-induced behaviors. *Cell* **137**, 949–960 (2009).
77. M. Dominguez, J. D. Wasserman, M. Freeman, Multiple functions of the EGF receptor in Drosophila eye development. *Curr. Biol.* **8**, 1039–1048 (1998).
78. S. Khare *et al.*, A KCNC3 mutation causes a neurodevelopmental, non-progressive SCA13 subtype associated with dominant negative effects and aberrant EGFR trafficking. *PLoS One* **12**, e0173565 (2017).
79. L. Aron *et al.*, Pro-survival role for Parkinson's associated gene DJ-1 revealed in trophically impaired dopaminergic neurons. *PLoS Biol.* **8**, e1000349 (2010).
80. C. Ling *et al.*, The apical transmembrane protein Crumbs functions as a tumor suppressor that regulates Hippo signaling by binding to Expanded. *Proc. Natl. Acad. Sci. U.S.A.* **107**, 10532–10537 (2010).
81. C. L. Chen *et al.*, The apical-basal cell polarity determinant crumbs regulates Hippo signaling in Drosophila. *Proc. Natl. Acad. Sci. U.S.A.* **107**, 15810–15815 (2010).
82. N. A. Grzeschik, L. M. Parsons, M. L. Allott, K. F. Harvey, H. E. Richardson, Lgl, aPKC, and Crumbs regulate the Salvador/Warts/Hippo pathway through two distinct mechanisms. *Curr. Biol.* **20**, 573–581 (2010).
83. P. Ribeiro, M. Holder, D. Frith, A. P. Snijders, N. Tapon, Crumbs promotes expanded recognition and degradation by the SCF(Slimb/beta-TrCP) ubiquitin ligase. *Proc. Natl. Acad. Sci. U.S.A.* **111**, E1980–1989 (2014).
84. N. A. Grzeschik, E. Knust, IrreC/rst-mediated cell sorting during Drosophila pupal eye development depends on proper localisation of DE-cadherin. *Development.* **132**, 2035–2045 (2005).
85. B. Miotto *et al.*, Chameau HAT and DRpd3 HDAC function as antagonistic cofactors of JNK/AP-1-dependent transcription during Drosophila metamorphosis. *Genes Dev.* **20**, 101–112 (2006).
86. J. A. Bosch, N. H. Tran, I. K. Hariharan, CoinFLP: A system for efficient mosaic screening and for visualizing clonal boundaries in Drosophila. *Development* **142**, 597–606 (2015).